Hindawi
Journal of Electrical and Computer Engineering
Volume 2022, Article ID 1237997, 25 pages
https://doi.org/10.1155/2022/1237997

Research Article

Effects of Conditional Changes on High-Voltage Direct Current Transmission Line Characteristic

Chaichan Pothisarn,[1] Atthapol Ngaopitakkul,[1] Monthon Leelajindakrairerk,[1] Natthanon Phannil,[1] Sulee Bunjongjit,[2] Surakit Thongsuk,[3] and Bancha Sreewirote[4]

[1]*School of Engineering, King Mongkut's Institute of Technology Ladkrabang, Bangkok, Thailand*
[2]*Faculty of Engineering, University of Technology Rattanakosin, Nakhon Pathom, Thailand*
[3]*Faculty of Industrial Technology, Rajabhat Rajanagarindra University, Chachoengsao, Thailand*
[4]*Faculty of Engineering, Thonburi University, Bangkok, Thailand*

Correspondence should be addressed to Atthapol Ngaopitakkul; knatthap@kmitl.ac.th

Received 15 November 2021; Revised 21 July 2022; Accepted 27 July 2022; Published 29 August 2022

Academic Editor: Bhargav Appasani

The high-voltage direct current (HVDC) transmission system, which links the Gurun Substation of the National Electric Authority of Malaysia (Tenaga Nasional Berhad, TNB) with the Khlong Ngae Station of the Electricity Generating Authority of Thailand (EGAT), has been extensively researched to achieve the highest quality because it is the largest of its kind in Thailand, and there is a plant to expand its transmission power. However, the impact on the whole system is under-researched. To study and develop this system, the HVDC transmission line is modelled with the MATLAB/Simulink program and a laboratory setup to investigate the effect of transmission line distance, load power, and voltage on power loss, voltage drop, and waveform. The HVDC transmission line parameters are calculated from the actual transmission line parameters and converted to the simulation model parameters using the per-unit method. The model is verified and tested by the simulation program before creating the experimental setup. The simulation and experimental results demonstrate the effects of changing system conditions via the three aspects. All the three conditions directly affect the HVDC transmission line; nevertheless, they affect each aspect differently.

1. Introduction

Currently, the high-voltage direct current (HVDC) transmission system is widely used because it has more advantages (such as low power loss, easy control of power flow, and long-distance power transmission) than the high-voltage alternating current (HVAC) transmission system. The technology of the HVDC transmission system is constantly evolving. Many countries adopt it to deliver a large amount of electricity. For example, the bipolar HVDC transmission system of the BritNed project connects power stations in Great Britain to those in the Netherlands. The BritNed project started in 2011 using a ±450 kV submarine cable with a capacity of 1,000 MW over a distance of 260 km. In the United States, the innovative HVDC PLUS transmission line technology from Siemens was first applied to the Trans Bay Cable Project. It can deliver both active and reactive powers of 400 MW and ±170 Mvar, respectively, with a voltage of ±200 kV. In India, there are many HVDC transmission systems, including the Ballia-Bhiwadi project (2,500 MW, ±500 kV, 800 km) and the Mundra-Haryana project (2,500 MW, ±500 kV, 960 km). From 2010, China has been the country with the largest use of the HVDC transmission system in Asia. It also has plans of building approximately 35 projects, totalling 217 GW of power transmission [1].

The EGAT-TNB HVDC transmission system has begun to play a more crucial role in Thailand. It is used to link the Gurun Substation of the National Electric Authority of Malaysia (Tenaga Nasional Berhad, TNB) with the Khlong Ngae Station of the Electricity Generating Authority of Thailand (EGAT). There exists another project that aims to

connect China to Thailand. Additionally, its usage will be expanded to cover its connection to distant or offshore alternative energy sources, such as wind and solar farms.

In recent times, alternative energy is widely used commercially, and the technology of energy production is being developed worldwide. According to the International Energy Agency (IEA), an average industrial growth of 40% over the past ten years has resulted in a variety of photovoltaic technology. The IEA estimates that photovoltaic power generation will account for 5% of global electricity by 2030 and increase to 11% by 2050. This will potentially reduce 2,300 million tons of carbon dioxide emissions per year. In India, the renewable energy trade is very successful because there are many large photovoltaic power plants. Most of them are connected to the grid system [2], and their transmission lines run over a very long distance because they are distant from the load centre. One of the longest HVDC transmission lines in the world is built in India to supply a capacity of 2,000 MW from Talcher to Tamil Nadu over 1,400 km. Likewise, the HVDC transmission system is used in many developing countries to reduce power loss in long-distance transmission lines [3–6].

In Thailand, the renewable energy capacity from 2013 to 2016 and its target in 2036 [7] in Table 1 show a continuous development of renewable energy production resulting from government policies. Among all the renewable energy types, the solar capacity has the largest increase. A solar power plant requires a large space; therefore, it must be built in a remote area. Power transmission over a long distance causes a significant power loss in the transmission line; nonetheless, if it is developed into the HVDC transmission line, the power loss will decrease substantially. Various aspects of the HVDC transmission system still need to be studied before they can be put into practice.

The HVDC power transmission system has been developed in various research fields. One of the important areas is the development of converters [8]. The essential devices can be categorized into two types: rectifiers and inverters [9]. The rectifier is installed at the sending side of the HVDC transmission line to convert AC to DC power. Alternatively, the inverter is installed at the receiving side to convert DC to AC power. At the beginning of the development, the line-commutated converter (LCC), also known as the current source converter (CSC), was popularly applied using the thyristor technology. This can support a high value of power, voltage, and current. Subsequently, a switching device, that is, the insulated-gate bipolar transistor (IGBT), that can quickly turn on and off was created. The IGBT was applied to develop a new converter type known as the voltage source converter (VSC) [10]. The VSC has more advantages than the LCC [11]. For example, the VSC can independently control both active and reactive powers; however, the LCC cannot control the reactive power [12]. Moreover, the VSC is smaller than the LCC because it does not need a trigger guard, and its filter is smaller [13]. A number of studies have focused on improving the performance of the VSC [14] and the LCC [15]. Furthermore, the fuzzy logic has also been applied to the control system to allow more power transmission. Recently, the multiterminal converter (MTC) has been developed to improve the overall efficiency of power transmission [16]. In addition, it has been developed by combining LCC and VSC as a hybrid HVDC system [17], which can take advantage of both converters. The hybrid HVDC system can be divided into 4 types: a pole hybrid HVDC system, a terminal hybrid HVDC system, a series hybrid HVDC system, and a parallel hybrid HVDC system.

The HVDC transmission system has been researched in several studies to deliver a large amount of electricity over a long distance and reduce power loss [18] in the HVDC transmission line. These studies have proposed a method for calculating the power loss in the HVDC transmission line. The computation of the entire system is very complex. Therefore, it is necessary to separate the power loss calculation from the converter station [19, 20] and the HVDC transmission line [20–23]. In a study by Jovcic [23], the power loss of each device in the HVDC transmission line using the VSC was calculated and simulated in two models. The first model (±150 kV, 350 MW, 100 km) had a power loss of 4.6%, whereas the second model (±300 kV, 1000 MW, 200 km) lost 4.9% of its power. The results suggested that the transmission line distance, voltage, and load power affected the power loss. Furthermore, a power loss arising from the corona phenomenon is calculated [24]; the current harmonics are considered and possibly analysed using the PSCAD/EMTDC program [25]. Most studies have been conducted to reduce the power loss in the HVDC transmission line by enhancing the functionality of the converter [26] and improving the transmission line connection [27].

Generally, the model of HVDC transmission systems should be selected to suit the analysis method. The most popular models are the π-equivalent circuit, T-equivalent circuit, universal line, and Bergeron circuit models [28–31]. Khatir studied the π-equivalent circuit model using the MATLAB/Simulink program [29, 32]. The π model is suitable for analysis at low frequencies [29], whereas the universal line model is most appropriate for underground and submarine cables [33–35]. Other researchers used different methods for calculating the transmission line parameters [36–47] and the PSCAD/EMTDC program based on the CIGRE Benchmark to study the simulation models.

In Thailand, studies on the HVDC transmission system have attracted scholarly attention. For example, the EGAT-TNB HVDC transmission system, which increases the stability of the network in Southern Thailand and connects the ASEAN network in the future project of "ASEAN Power Grid," was studied using the ATP program to control powers. It was also used to analyse fault events [48–53], fault signals [54–56], and fault location [57]. The power flow of this system was analysed using dynamic simulation to validate the stability and reliability of the operation of the HVDC transmission line [58–63].

However, the simulations in these studies were done using computer programs, which might differ from the actual electrical system. The EGAT-TNB HVDC transmission system should be extensively researched, making it efficient both theoretically and practically. Therefore, this study focuses on the possibility and impact of changing the

Table 1: Renewable energy capacity from 2013 to 2016 and its target in 2036 [7].

Renewable energy	Capacity (MW)				
	2013	2014	2015	2016	Target of 2036
1. Solar power	823.46	1298.51	1419.58	2146.00	6000.00
2. Wind power	222.71	224.47	233.90	305.74	3002.00
3. Small hydropower	108.80	142.01	172.12	182.08	376.00
4. Biomass	2320.78	2451.82	2726.60	2811.89	5570.00
5. Biogas	265.23	311.50	372.51	421.77	1280.00
6. Garbage	47.48	65.72	131.68	145.28	550.00
7. Large hydroenergy	—	—	2906.40	2906.40	2906.40
Total	**3788.46**	**4494.03**	**7962.79**	**8919.16**	**19684.40**

relevant factors in the HVDC transmission line. In this research, the EGAT-TNB HVDC transmission line is modelled using the MATLAB/Simulink program and a laboratory setup to study the effects of transmission line distance, transmission line voltage, and load power on power loss, voltage drop, and waveform. The simulation and experimental results can be used to predict the impacts and prevent possible damage. In the future, this system will be studied on the topic of renewable energy connections and faults in HVDC transmission lines. Some electrical parameters cannot be studied through the simulation model only, so a comparative study of both the computer program and the laboratory setup is needed. This study is beneficial to researchers, government agencies, students, and those interested in the HVDC transmission system.

The contributions of this study are summarized as follows:

(1)This paper studies the possibility of simulating the real HVDC transmission line system to be the HVDC transmission line experiment setup in the laboratory

(2)This paper designs the HVDC transmission line model in both the computer program and the experimental setup to determine the accuracy and use it as a tool for further analysis of electrical characteristics

(3)This paper studies the effect of the transmission line distance, size load, and voltage on power loss, voltage drop, and waveform using the MATLAB/Simulink program and the experimental setup for consideration of preventing damage to the HVDC system

This study is organized as follows: Section 2 explains the HVDC transmission line that is designed in MATLAB/Simulink and applied to the experimental setup; Section 3 highlights the results of the simulation and the experimental setup in three subsections according to the conditions; and finally, Section 4 concludes the study.

2. Design of the Simulation Model and the Experimental Setup

The HVDC transmission system in this study is modelled after a real system. The system links the Gurun Power Station of the Tenaga Nasional Berhad (TNB) to the Khlong Ngae Power Station of the Electricity Generating Authority of Thailand (EGAT). The HVDC transmission line structure is a monopolar model with a metallic power return path as shown in Figure 1.

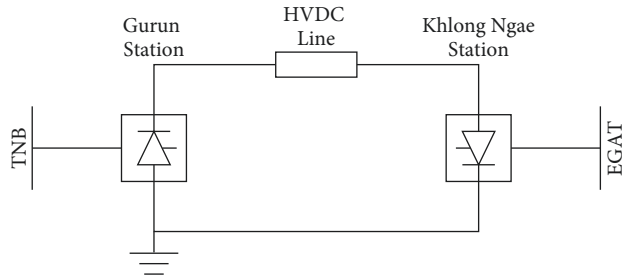

Figure 1: Monopolar HVDC transmission system with a metallic power return path.

This system is studied using both a simulation model and an experimental setup. In the simulation model, the MATLAB/Simulink program is used to simulate the HVDC transmission system. The effect of the change in the transmission line distance, load power, and voltage on power loss, voltage drop, and waveform is observed. The simulation model and results are applied to design the experimental setup in a laboratory room to confirm that the results can be practically used.

2.1. Simulation Model Design Using MATLAB/Simulink Program. The EGAT-TNB HVDC transmission line is modelled in the MATLAB/Simulink program to compare the simulation results with actual data and with other studies to validate the system design and verify its reliability. This simulation is divided into two steps: First, the parameters of the EGAT-TNB HVDC transmission line are calculated using the per-unit method to assemble the simulation model and to assess the reliability of the circuit model; and second, the model is customized based on the experimental setup.

2.1.1. Simulation to Verify Reliability. This study uses a simple 6-pulse 250 kV 500 MW HVDC transmission system model [64] as the base model in the MATLAB/Simulink program as shown in Figure 2(a). A 315 kV 5000 MVA alternating current source supplies the power via an electric filter and a 315/210 kV 600 MVA transformer to a rectifier. The rectifier uses thyristor switching devices to convert AC to DC power. A current regulator with a PI controller is used

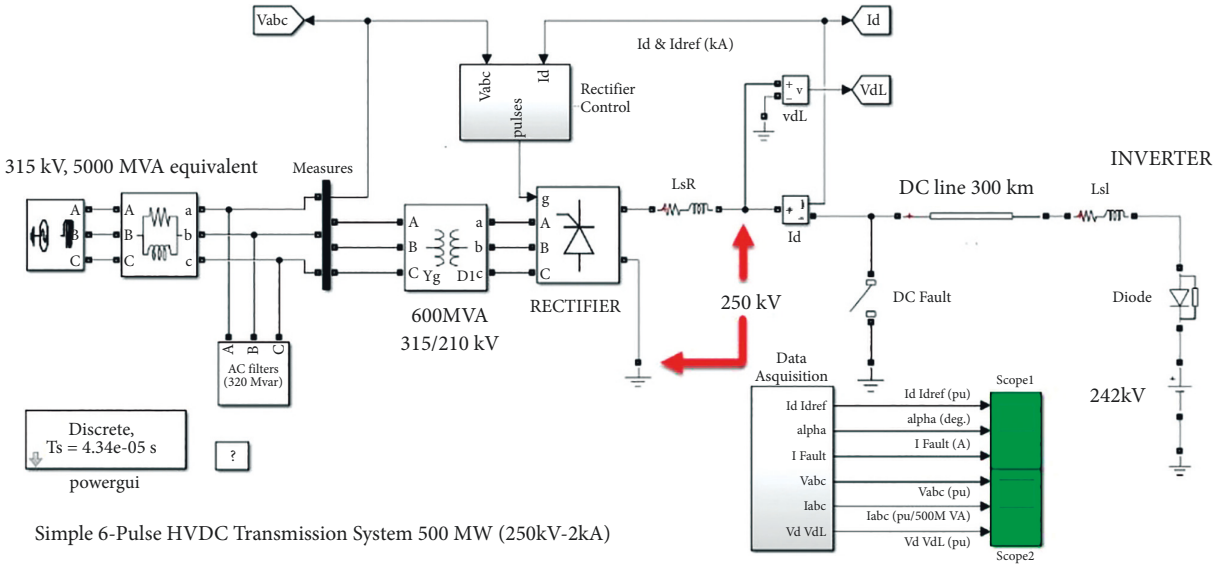

Simple 6-Pulse HVDC Transmission System 500 MW (250kV-2kA)

(a)

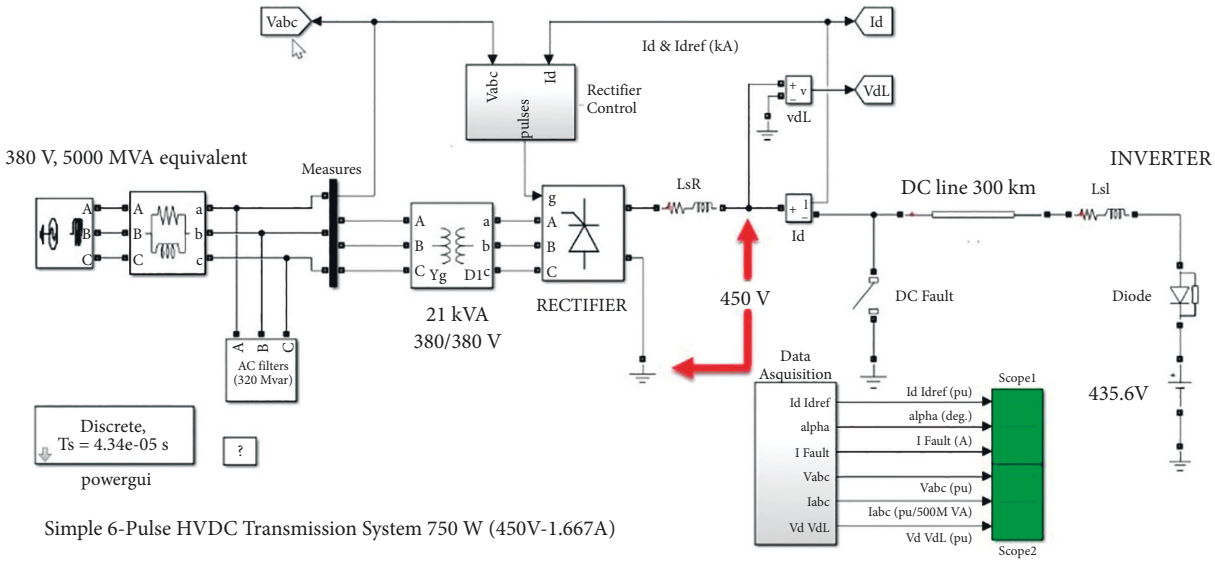

Simple 6-Pulse HVDC Transmission System 750 W (450V-1.667A)

(b)

Figure 2: Continued.

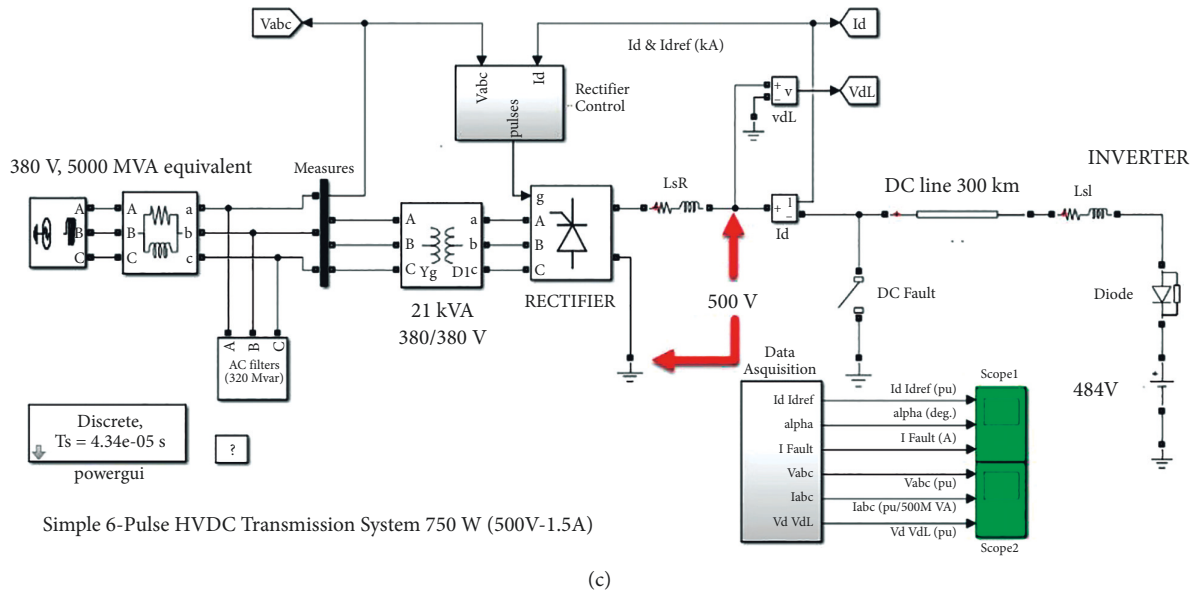

(c)

Figure 2: Simulation models of HVDC transmission systems. (a) Circuit model of a 250 kV HVDC transmission system (250 kV, 500 kVA, 2 kA), (b) circuit model of a 450V HVDC transmission system (450 V, 750 VA, 1.667 A), and (c) circuit model of a 500V HVDC transmission system (500 V, 750 VA, 1.5 A).

Table 2: Parameter of the actual and design systems.

Position	Parameter	Actual system	450 V system	500 V system
Sending side	DC voltage (kV)	250.000	0.450	0.500
	DC current (A)	2000.000	1.667	1.500
	Active power (kW)	500.000	0.750	0.750
Transmission line	Resistance (Ω/km)	0.015	0.014	0.017
	Inductance (mH/km)	0.792	0.713	0.880
	Capacitance (nF/km)	14.400	16.000	12.960
Receiving side	DC voltage (kV)	242.000	0.437	0.484
	AC voltage (kV)	210.000	0.380	0.380

in the rectifier control to control the trigger angle (alpha). The parameters: resistance (R), inductance (L), and capacitance (C), are calculated from the real HVDC transmission line with a distance of 300 km. Insulated-gate bipolar transistors (IGBT) are employed in an inverter to convert the power from DC to AC. The inverter uses a pulse width modulation (PWM) controller and an optimal modulation index to keep a constant output voltage.

The test of the experimental setup has a limit on the electrical capability. The voltage, current, and power must be within the range of safety controls, and it is impossible to create the experimental setup based on a 250 kV simple model. We choose 450 V and 500 V design models for testing and building the experimental setup as shown in Figures 2(b) and 2(c). This is because both voltages are close to the common laboratory voltage and high enough for the test to show obvious effects. The design models employ parameters transformed from the 250 kV simple model by the per-unit method according to Table 2. The powers of both design models are limited to a capacity of 750 W.

To ensure the reliability of a base model and both design models, they are tested under five conditions to study the response characteristics of the system in each system change condition. The test is divided into 5 conditions: a low current operation, a normal operation, a fault situation, a trigger angle change, and a normal operation. The simulation results are shown in terms of current, alpha angle, fault current, and voltage in Figures 3–6, respectively. Each figure compares the results of the three systems: 250 kV, 450 V, and 500 V models. First, when the system responds to a low-current operation in ranges of 0 to 0.3 s, the reference current is set at a constant value of 0.5 pu. In Figure 3, the 250 kV, 450 V, and 500 V models reach their respective steady states at 0.1, 0.075, and 0.055 s, respectively, whereas all of their trigger angles are approximately 60°. Second, when the system responds to a normal operation during 0.3 to 0.5 s, the reference current is set to 1.1 pu. The response current takes approximately 0.13, 0.1, and 0.075 s, respectively, to enter a new steady state. In Figure 4, the trigger angle decreases from 60 to 45, 50, and 50°, respectively, but there is no change in fault current and voltage, shown in

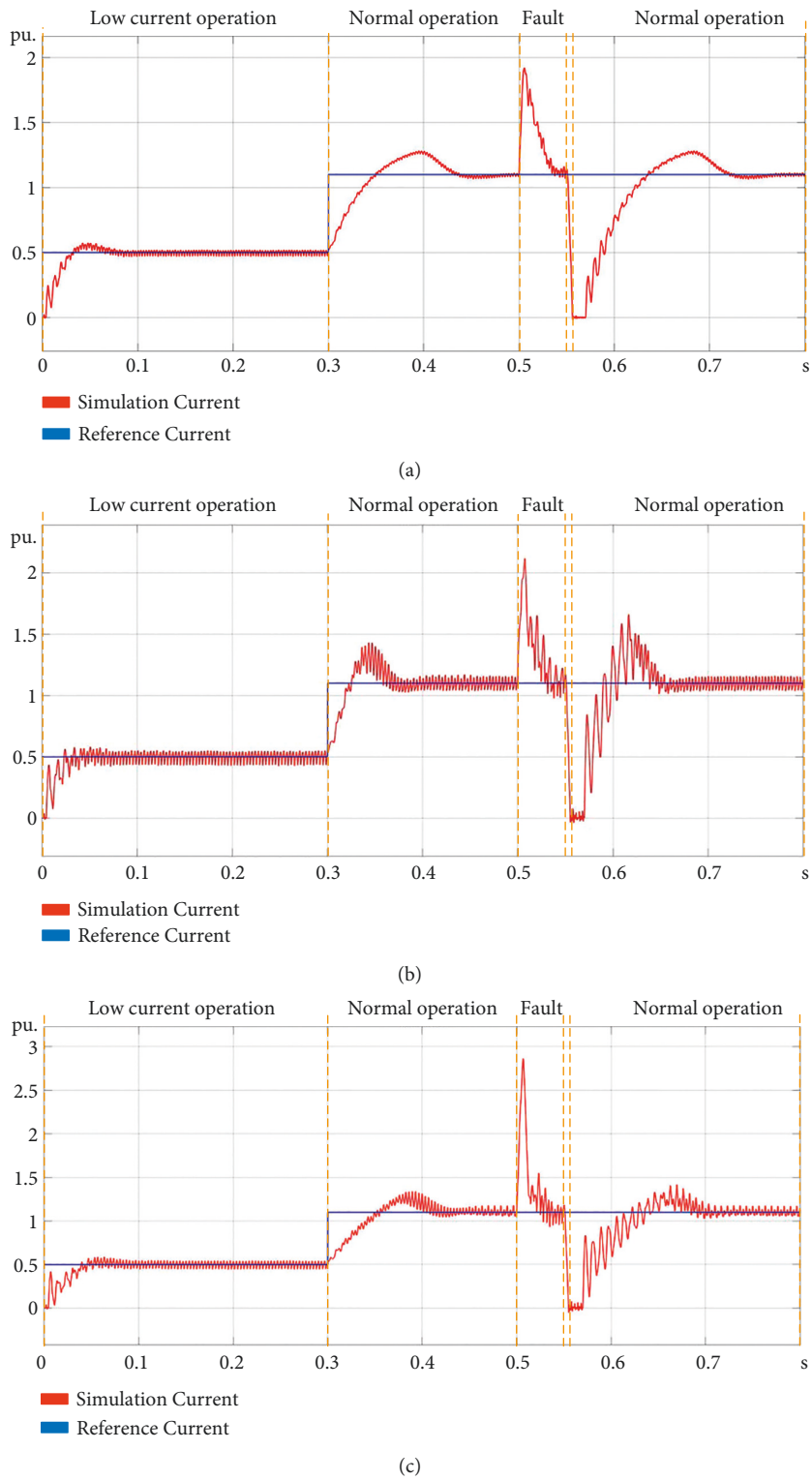

Figure 3: Current of the HVDC transmission line. (a) A 250 kV HVDC transmission line (250 kV, 500 kVA, 2 kA), (b) a 450 V HVDC transmission line (450 V, 750 VA, 1.667 A), and (c) a 500 V HVDC transmission line (500 V, 750 VA, 1.5 A).

Figures 5 and 6. Third, after a fault occurs in the system at 0.5 s, the respective maximum fault current is approximately 5 kA, 6 A, and 5 A as shown in Figure 5, respectively. Fourth, during the interval from 0.55 to 0.57 s, the trigger angle that is forced by the protection system is changed to 165°. Thus, the rectifier operates in the inverter mode and delivers power back to the power source, and the fault current is eliminated from the system. Finally, between 0.57 and 0.8 s, the system resumes its normal operation and enters a steady state at 0.75, 0.67, and 0.67 s,

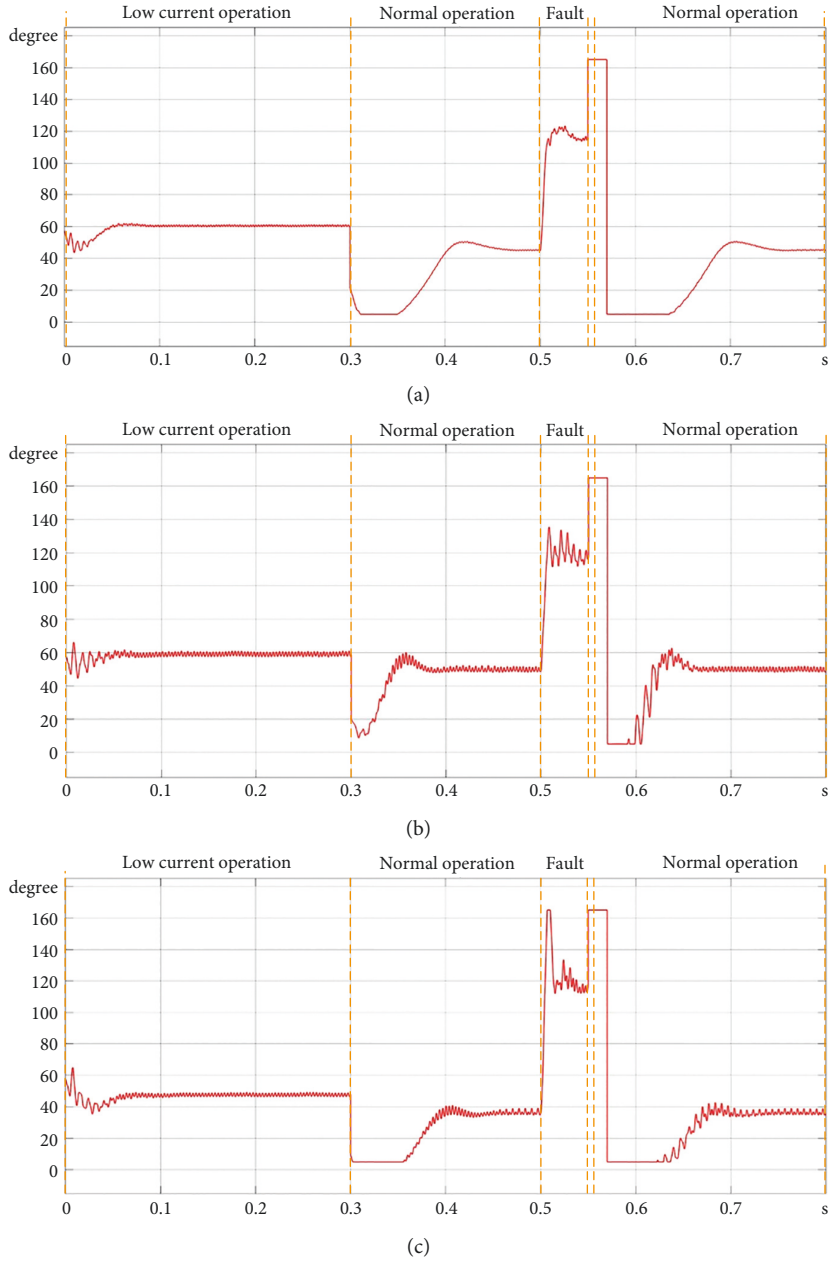

Figure 4: Alpha angle of the HVDC transmission line. (a) A 250 kV HVDC transmission line (250 kV, 500 kVA, 2 kA), (b) a 450 V HVDC transmission line (450 V, 750 VA, 1.667 A), and (c) a 500 V HVDC transmission line (500 V, 750 VA, 1.5 A).

respectively. The system's responses to all 5 conditions are similar in direction and time responses. This makes it possible to conclude that both the 450 V and 500 V models can be used to represent the 250 kV model. Therefore, the experimental setup is designed based on both models, which are presented in the next subsection.

2.2. Experimental Setup

2.2.1. Simulation for Experimental Setup with the MATLAB Program. The simulation model of the experimental setup is designed based on the 450 V and 500 V models; nevertheless, each device circuit is condensed into a device box for easy understanding as shown in Figure 7(a) and 7(b). The main devices in Table 3 and Figures 7(c)–7(h) consist of a power source, a transformer, a rectifier, an HVDC transmission line, an inverter, and an electrical load. The power source is set to a voltage of 380 volts and 50 Hz with an internal resistance of 0.8929 ohms and an internal inductance of 6×10^{-3} henries to simulate according to the laboratory's electrical system as shown in Figure 7(c). In Figure 7(d), the electrical power from the power source is supplied to a 21 kVA 380/380 V transformer. It is then sent to the rectifier in Figure 7(e) to convert AC power to DC power for supplying the transmission line. The rectifier has a circuit for

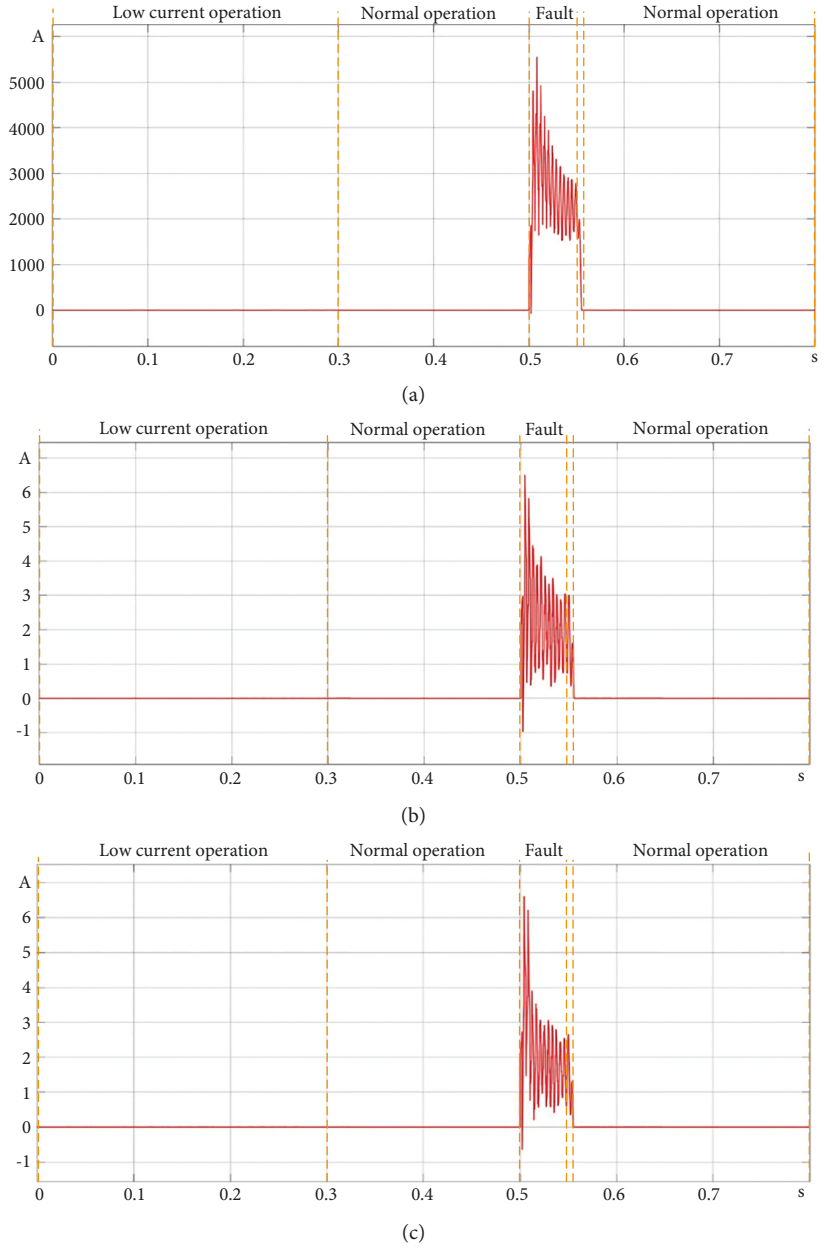

Figure 5: Fault current of the HVDC transmission line. (a) A 250 kV HVDC transmission line (250 kV, 500 kVA, 2 kA), (b) a 450 V HVDC transmission line (450 V, 750 VA, 1.667 A), and (c) a 500 V HVDC transmission line (500 V, 750 VA, 1.5 A).

controlling the alpha angle, which can control the amount of power supply of the system. The rectifier output voltage is set to 450 V and 500 V according to the designed model. Electrical power is transmitted through the transmission line model that is simulated using resistors, inductors, and capacitors as shown in Figure 7(f). They are arranged in the form of 2 pi circuits. Once the electricity goes through the transmission line, it is sent to the inverter to convert back to AC power and supplied to the load as shown in Figures 7(g) and 7(h). In this test, the electrical parameter is measured at two points. The sending and receiving sides of the HVDC transmission line are measured as shown in Figure 7(b) to study the effect of the transmission line distance, load power, and voltage on power loss, voltage drop, and waveform. The simulation results are shown in Section 3 and compared with the experimental results.

2.2.2. Experimental Setup Design. The experimental setup is built using a π-equivalent circuit in the HVDC transmission line as shown in Figure 8(a). It consists of an adjustable three-phase transformer, an electrical protection device, a rectifier, two DC circuit breakers, an HVDC transmission line, a three-phase inverter, and an electrical load. The three-phase power supply sends electric power through the AC circuit breaker to the adjustable three-phase transformer ① and the electrical protection device ②, respectively. This power is supplied from the protection device to the rectifier

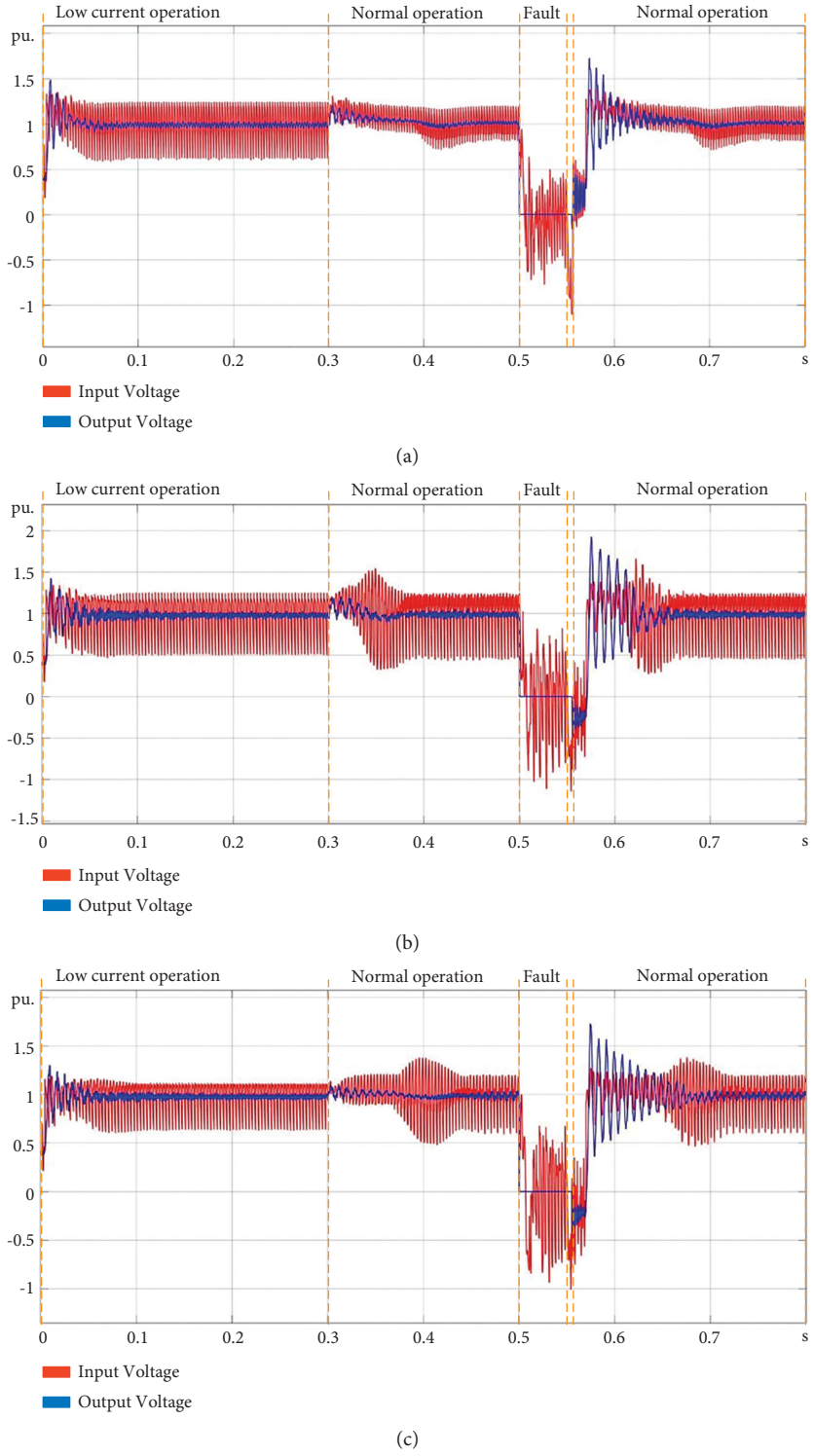

Figure 6: Voltage of the HVDC transmission line.

③, which converts electricity from AC to DC power before supplying it to the HVDC transmission line ⑤. The sending and receiving sides of the HVDC transmission line are controlled by the two DC circuit breakers ④ to protect both converters. Thereafter, at the end of the HVDC transmission line, there is a three-phase inverter ⑥, which inverts DC to AC power for supplying the electrical load ⑦. The parameters of the HVDC transmission line are adjusted by 12 selector switches as shown in Figures 8(b) and 8(d).

At two experimental measurement points, the sending and receiving sides, the effects on power loss, voltage drop, and waveform owing to transmission line distance, load

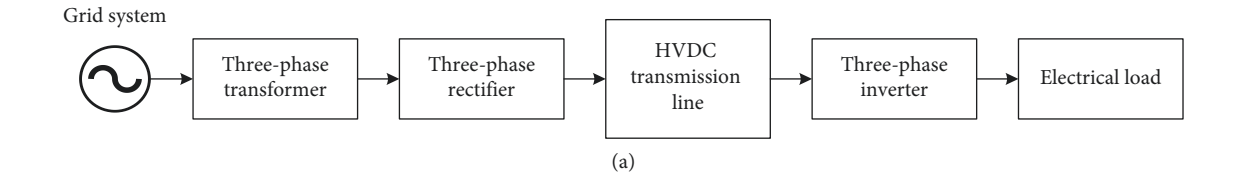

(a)

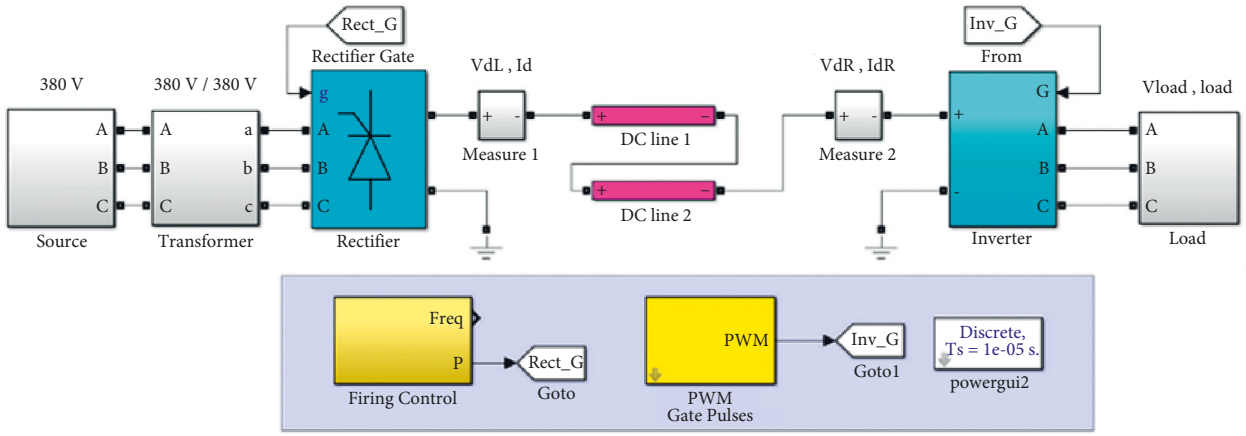

(b)

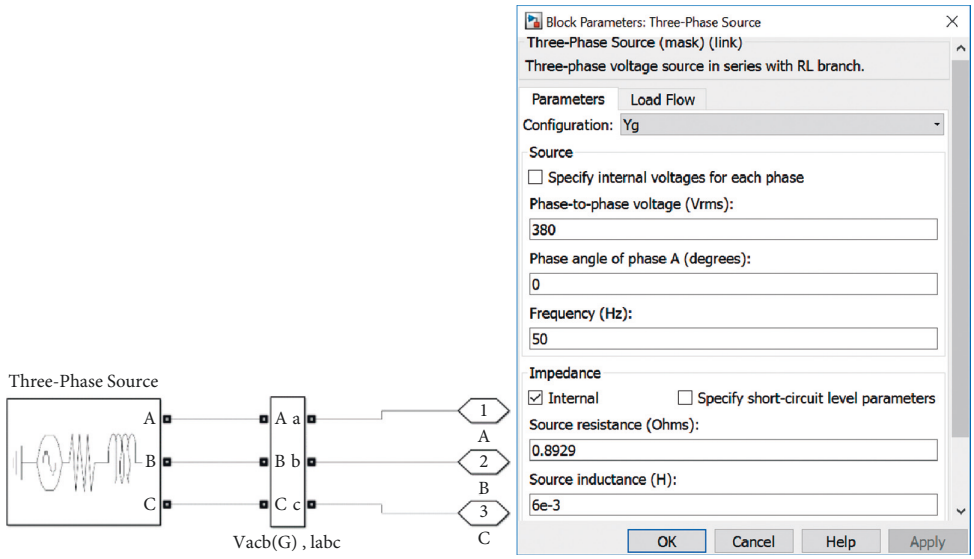

(c)

Figure 7: Continued.

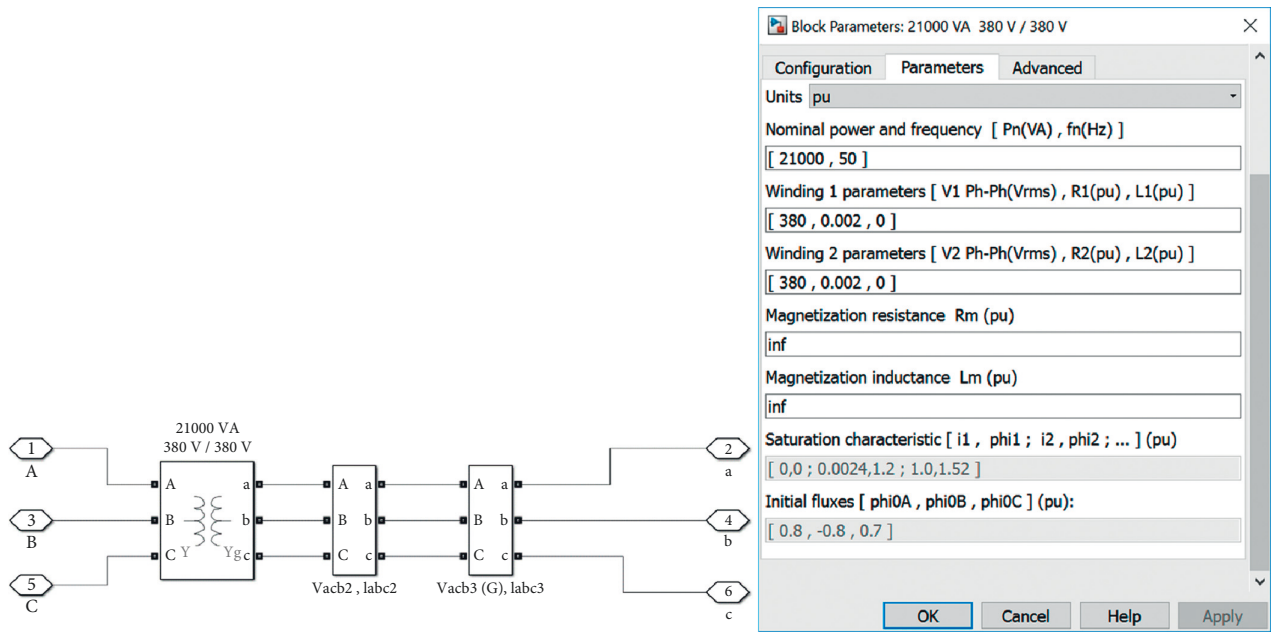

(d)

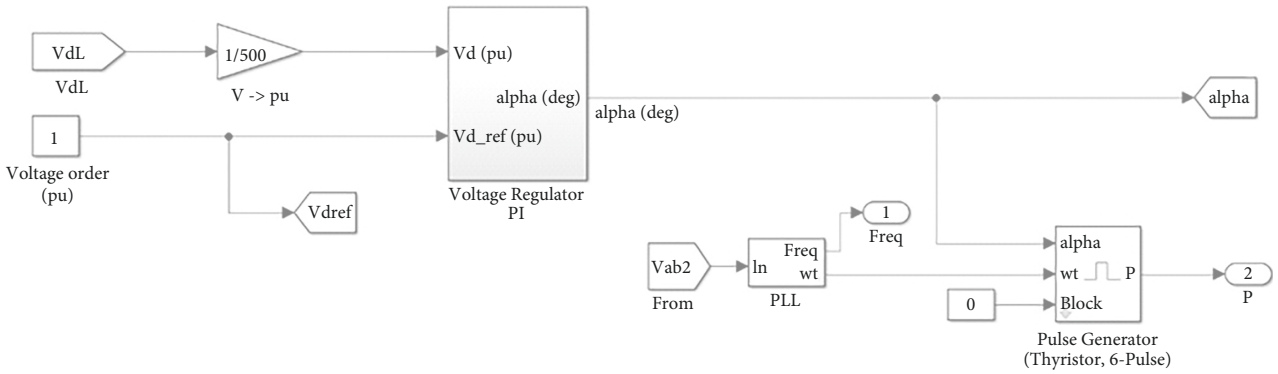

(e)

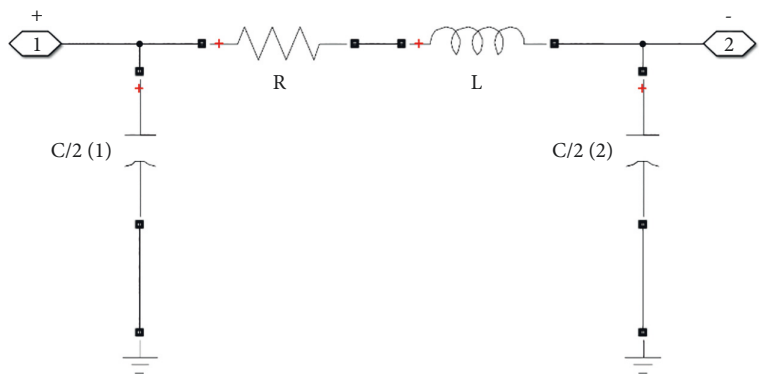

(f)

Figure 7: Continued.

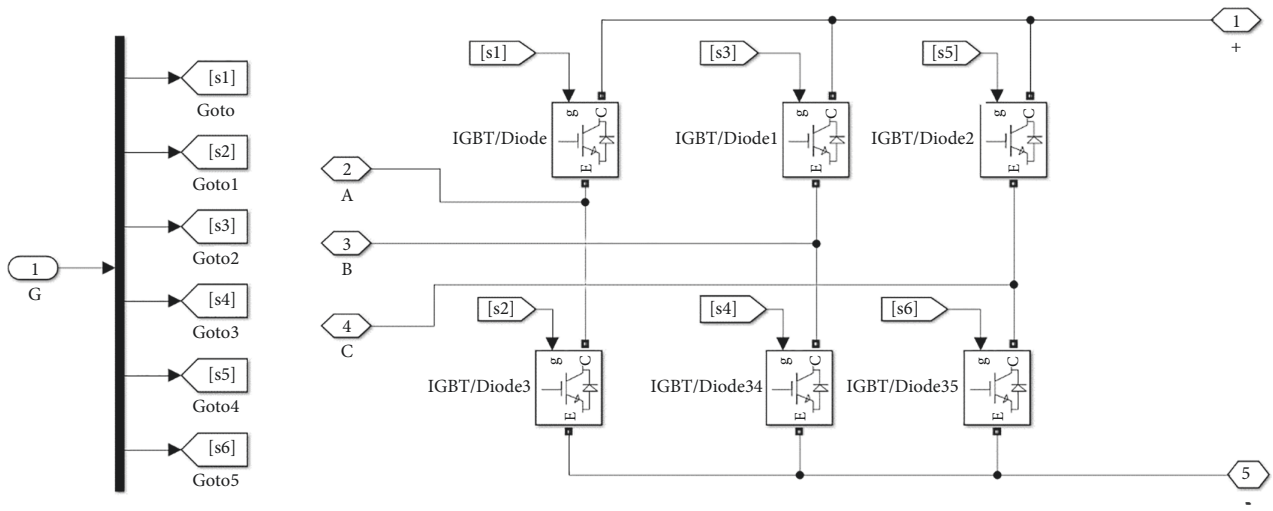

(g)

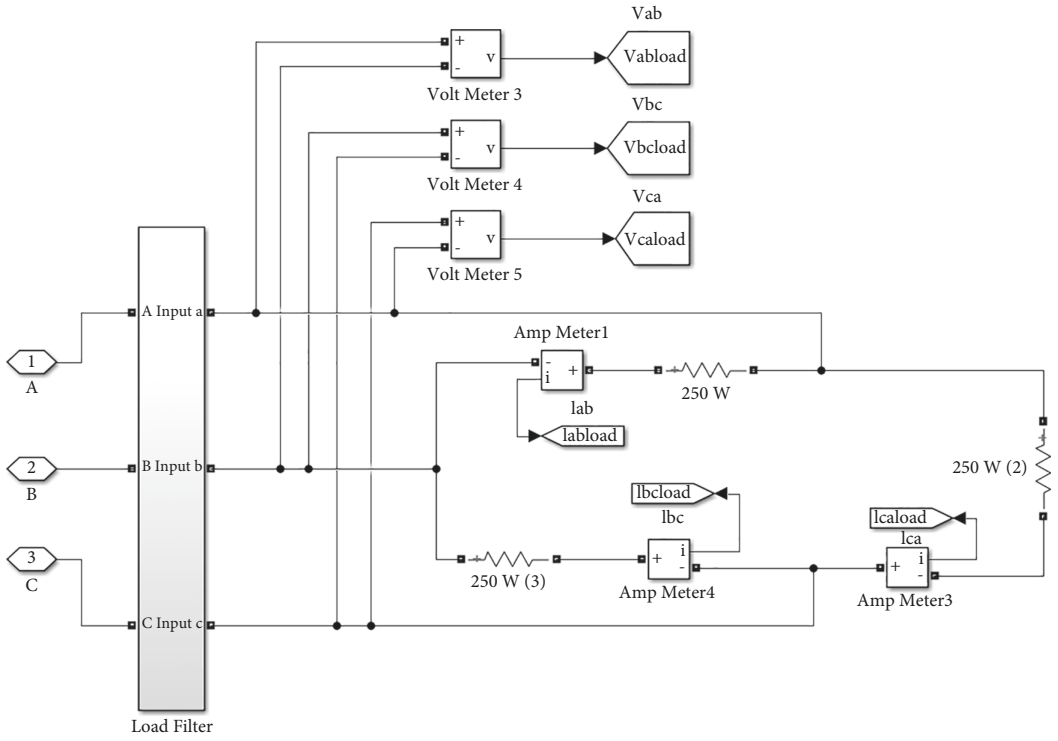

(h)

Figure 7: Model of the HVDC transmission line based on the experimental setup. (a) One-line diagram, (b) simulation model, (c) diagram and setup of the electric source block, (d) diagram and setup of the transformer block, (e) diagram and setup of the rectifier block, (f) diagram of the HVDC transmission line block, (g) diagram and setup of the inverter block, and (h) diagram and setup of the load block.

Table 3: Specification of the designed models.

Devices	Specification
AC source	380 V 50 Hz (star wiring)
Transformer	380/380 V 21 kVA (star-star wiring)
Rectifier	380 Vac/450–500 Vdc
HVDC transmission line	450–500 Vdc (2 pi circuits)
Inverter	450–500 Vdc/380 Vac
Load	250 VA 380 V (delta wiring)

power, and voltage are measured using the Fluke 435 Series II Basic Power Quality, Energy Analyser, and Teledyne LeCroy WaveSurfer 3024 as shown in Figure 8.

The parameters of the experimental setup are simulated from the parameters of the actual system. The resistance of the experimental setup is calculated by (1) [36] and converted using the per-unit method and used in the adjustable resistor as shown in Figure 9. The resistance is calculated in different voltages and distances as shown in Table 4. The transmission line circuit is divided into two parts (two pi

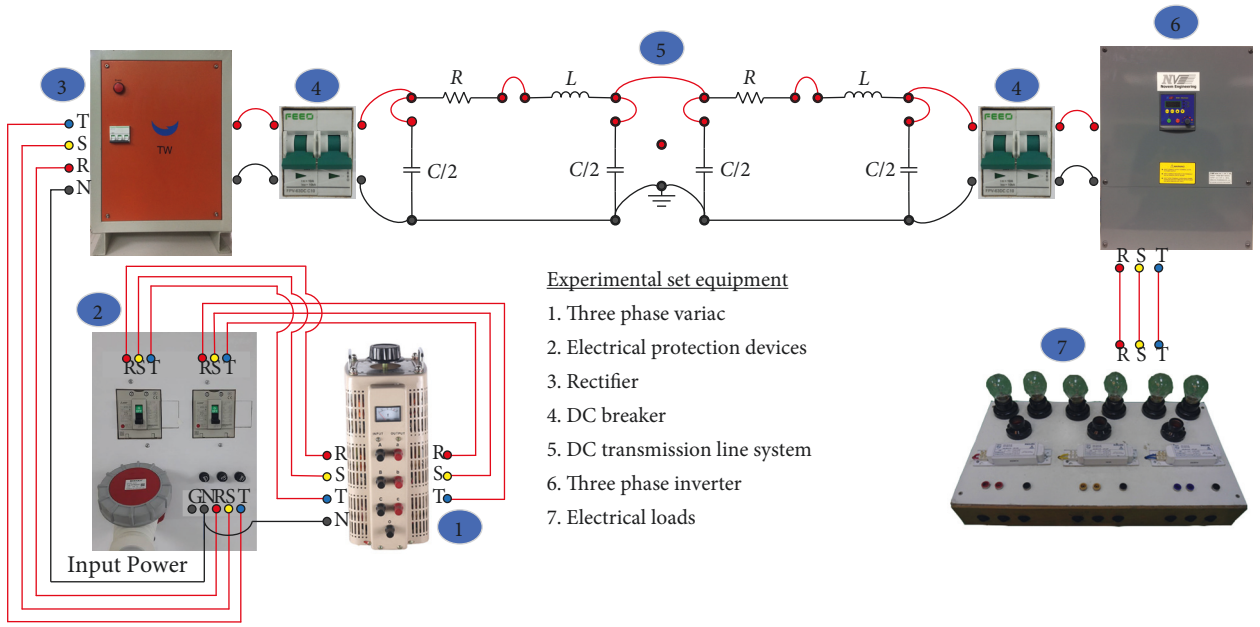

(a)

(b)

Figure 8: Continued.

(c)

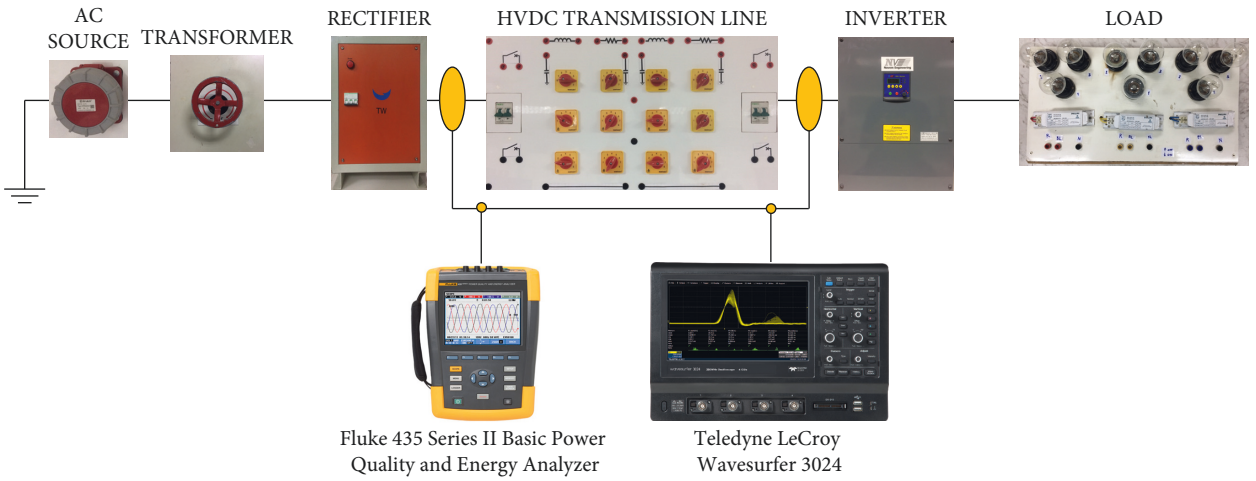

(d)

Figure 8: Experimental setup of the HVDC transmission line. (a) Schematic diagram of the experimental setup, (b) experimental setup, (c) behind the experiment setup, and (d) measurement points of the experimental setup.

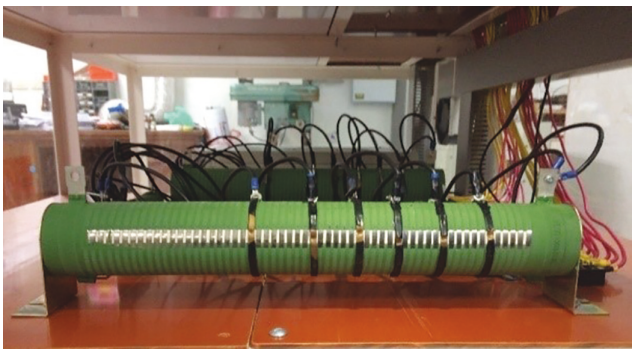

Figure 9: Resistors of the HVDC transmission line.

Table 4: Resistance of the HVDC transmission line model at different voltages and distances.

Voltage (V)	Distance (km)	Percentage of distance (%)	Resistance (Ω)		
			Calculation	Model system	Actual system
450	150	50	1.012	1.00	1.125
	300	50	2.025	2.00	2.250
	600	50	4.050	4.00	4.500
500	150	50	1.250	1.25	1.125
	300	50	2.500	2.50	2.250
	600	50	5.000	5.00	4.500

Figure 10: Inductors of the HVDC transmission line.

Table 5: Inductance of the HVDC transmission line model at different voltages and distances.

Voltage (V)	Distance (km)	Percentage of distance (%)	Inductance (mH)		
			Calculation	Model system	Actual system
450	150	50	53.46	53	59.4
	300	50	106.92	107	118.8
	600	50	213.84	214	237.6
500	150	50	66.00	65	59.4
	300	50	132.00	130	118.8
	600	50	264.00	260	237.6

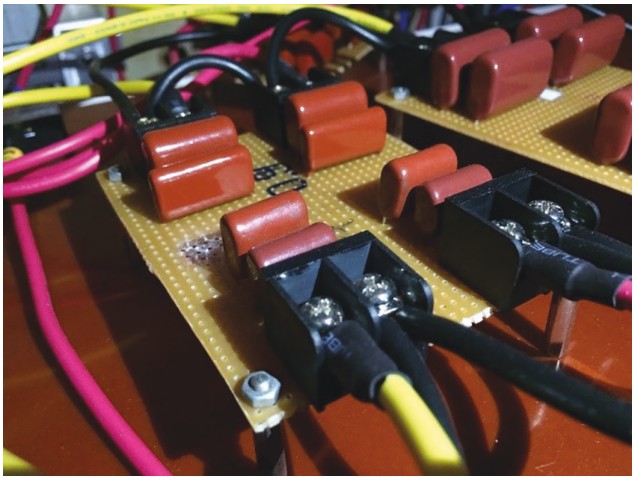

Figure 11: Capacitors of the HVDC transmission line.

circuit models). The sum of the parameters of both parts must be exactly the same as the HVDC transmission line value. Therefore, in the experiment setup, the resistance of each part is set as 50% of the HVDC transmission line value according to Figure 8(a) and Table 4.

$$r = \frac{\omega_1^2 K_2 - \omega_2^2 K_1}{\omega_2^2 - \omega_1^2}. \quad (1)$$

Here, r is an HVDC transmission line resistance (ohm/km), ω is a resonance frequency, and K is a computational constant.

The inductor of the experimental setup is made in the form of an adjustable inductor as shown in Figure 10. The inductance of the system is calculated using (2) [36]. Each inductance of the inductor in Table 5 is connected to the selector switch of the experimental setup to be used as the

Table 6: Capacitance of the HVDC transmission line model at different voltages and distances.

Voltage (V)	Distance (km)	Percentage of distance (%)	Inductance (mH)		
			Calculation	Model system	Actual system
450	150	25	0.30	0.30	2.7
	300	25	0.600	0.60	5.4
	600	25	1.200	1.20	10.8
500	150	25	0.243	0.27	2.7
	300	25	0.486	0.49	5.4
	600	25	0.972	1.00	10.8

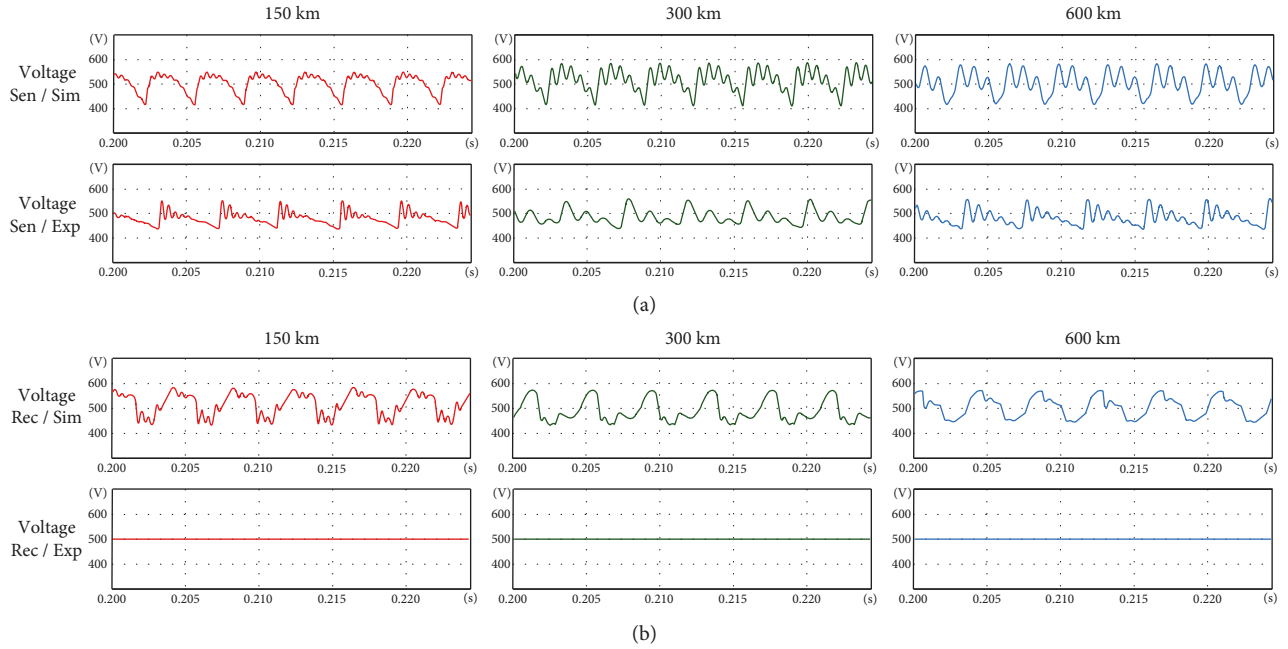

Figure 12: Comparison of the voltage waveforms based on the transmission line distance conditions. (a) Comparison of the sending side voltage waveforms and (b) comparison of the receiving side voltage waveforms.

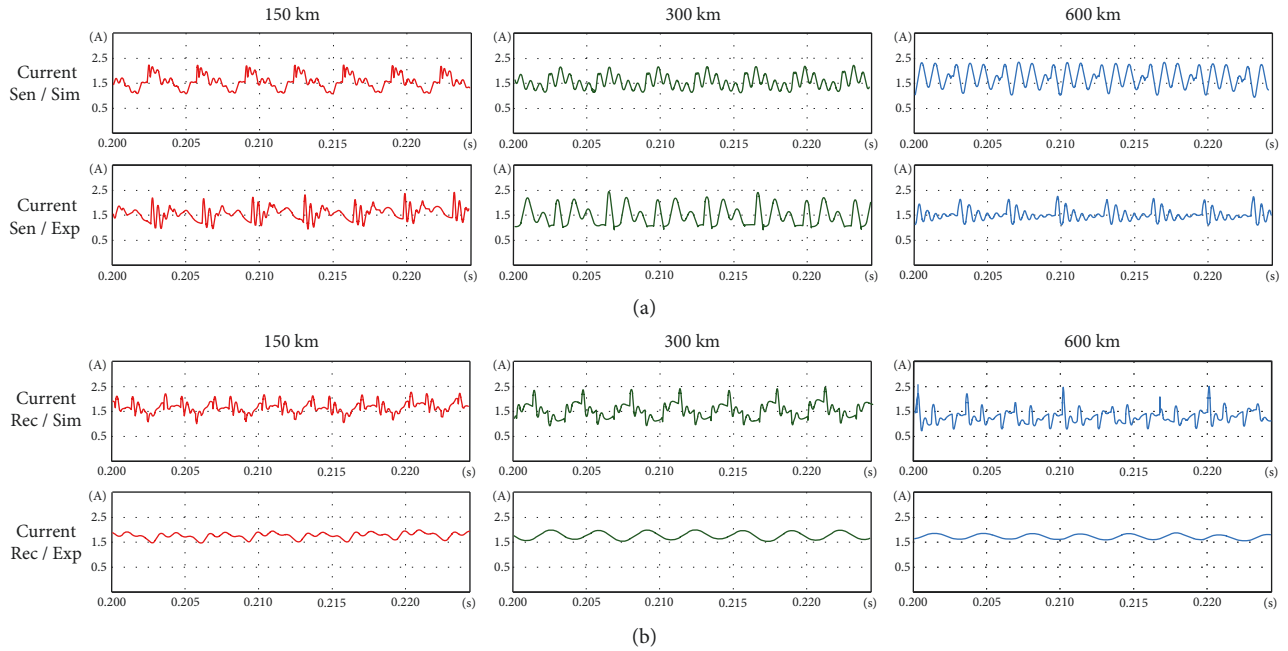

Figure 13: Comparison of the current waveforms based on the transmission line distance conditions. (a) Comparison of the sending side current waveforms and (b) comparison of the receiving side current waveforms.

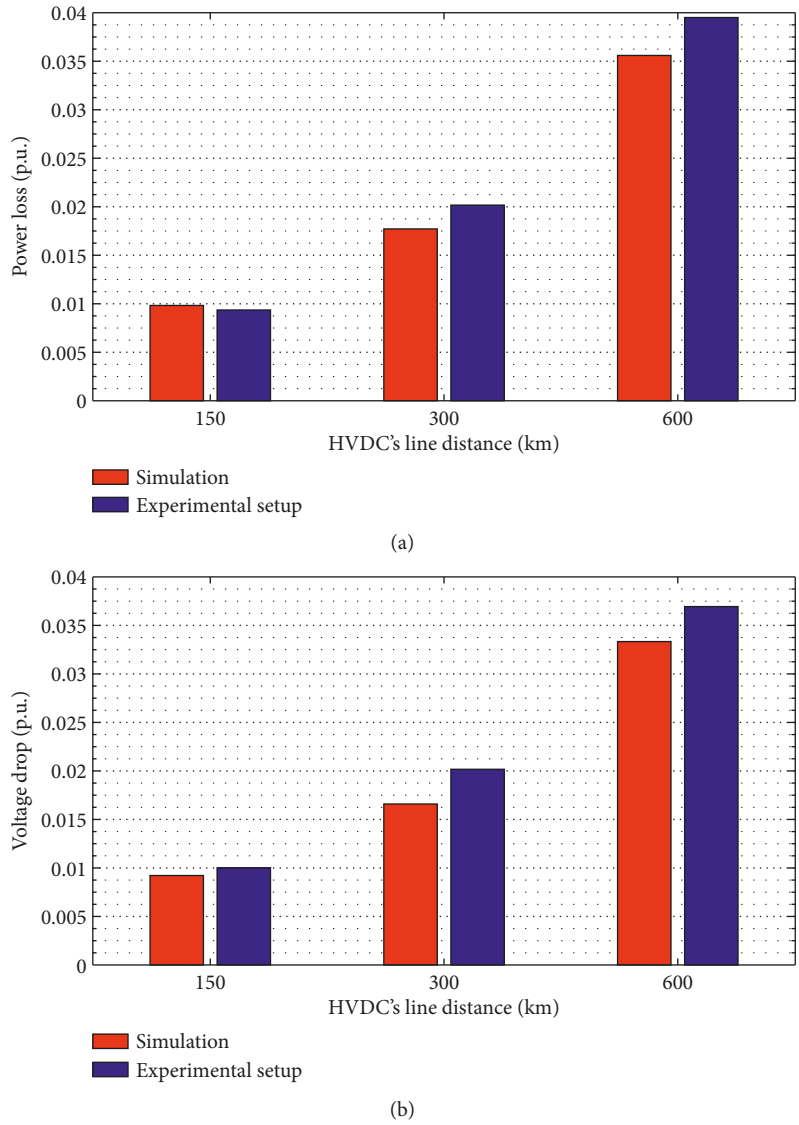

Figure 14: Comparison of the current waveforms based on transmission line distance conditions. (a) Comparison of the power losses and (b) comparison of the voltage drops.

HVDC transmission line parameter. Similar to the resistance, the transmission line circuit is divided into two parts, and the inductance of each part is set as 50% of the HVDC transmission line value according to Figure 8(a) and Table 5.

$$l = \frac{2R_{ch} + 2rL_{\text{line}} + rgL_{\text{line}}^2 R_{ch} - \omega_0^2 R_{ch} L_{\text{line}}^2 K_2 - K_1/\omega_2^2 - \omega_1^2}{2\omega_0^2 R_{ch} C_{ch} L_{\text{line}}}. \quad (2)$$

Here, l is an HVDC transmission line inductance (henry/km), r is an HVDC transmission line resistance (ohm/km), g is an HVDC transmission line conductance, ω is a resonance frequency, K is a computational constant, L_{line} is a line length (km), R_{ch} is a load resistance (ohm), and C_{ch} is a load capacitance (farad).

For the capacitance of the experimental setup in Figure 11, the film capacitor that can support a voltage of 630 V is selected to connect between the line and the neutron of the HVDC transmission line. The transmission line circuit is divided into two parts, and each part has two sides of the capacitor. Therefore, the capacitance of each side is set to be 25% of the HVDC transmission line value, making the sum of all the sides the same as the HVDC transmission line value as shown in Table 6. The capacitance of the HVDC transmission line is calculated according to (3) [36]. Each capacitance of the capacitor is also connected to the selector switch of the experimental setup to be used as the HVDC transmission line parameter.

$$c = \frac{1}{l} \frac{K_2 - K_1}{\omega_2^2 - \omega_1^2}. \quad (3)$$

Here, c is an HVDC transmission line capacitance (farad/km), l is an HVDC transmission line inductance (henry/km), ω is a resonance frequency, and K is a computational constant.

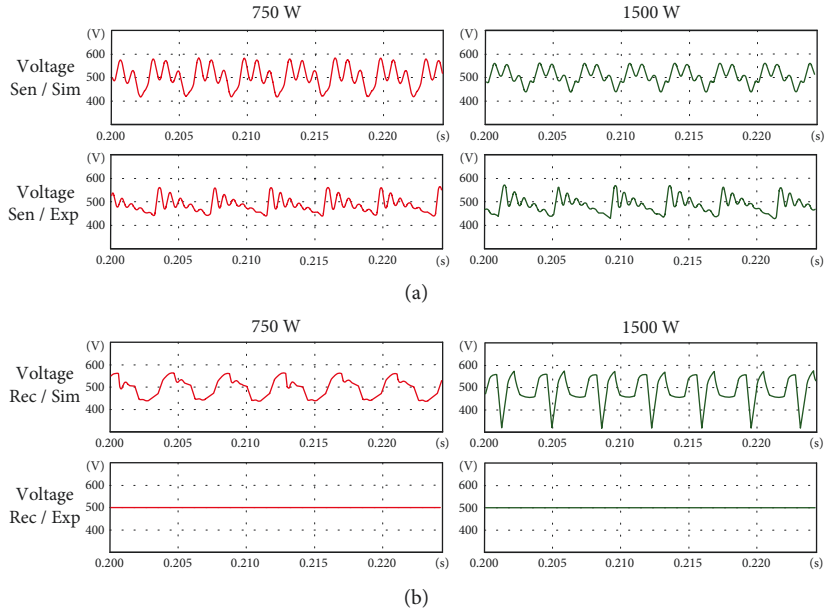

Figure 15: Comparison of the voltage waveforms based on the electrical load conditions. (a) Comparison of the sending side voltage waveforms and (b) comparison of the receiving side voltage waveforms.

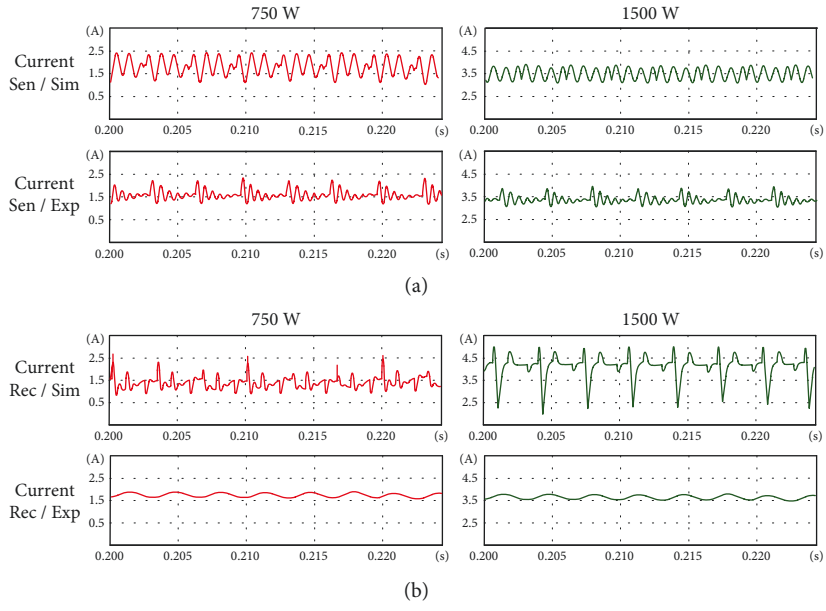

Figure 16: Comparison of the current waveforms based on the electrical load conditions. (a) Comparison of the sending side current waveforms and (b) comparison of the receiving side current waveforms.

3. Results of Simulation and the Experimental Setup

The EGAT-TNB HVDC transmission line is remodelled and tested in the MATLAB/Simulink program (Sim) and the experimental setup (Exp). The results are analysed in three subsections according to the varied conditions: transmission line distance, load, and voltage. The impacts on power loss and voltage drop are compared between the simulation and the experimental setup results.

The power loss and voltage drop are important parameters in evaluating the HVDC transmission line efficiency. The difference in power loss and voltage drop between the source and destination of the HVDC transmission line is presented to compare the resulting changes as shown in [65]

$$P_{\text{loss,line}} = P_{\text{Sen}} - P_{\text{Rec}}, \tag{4}$$

$$P_{\text{loss,line}} = G\left(V_{\text{drop,line}}\right)^2, \tag{5}$$

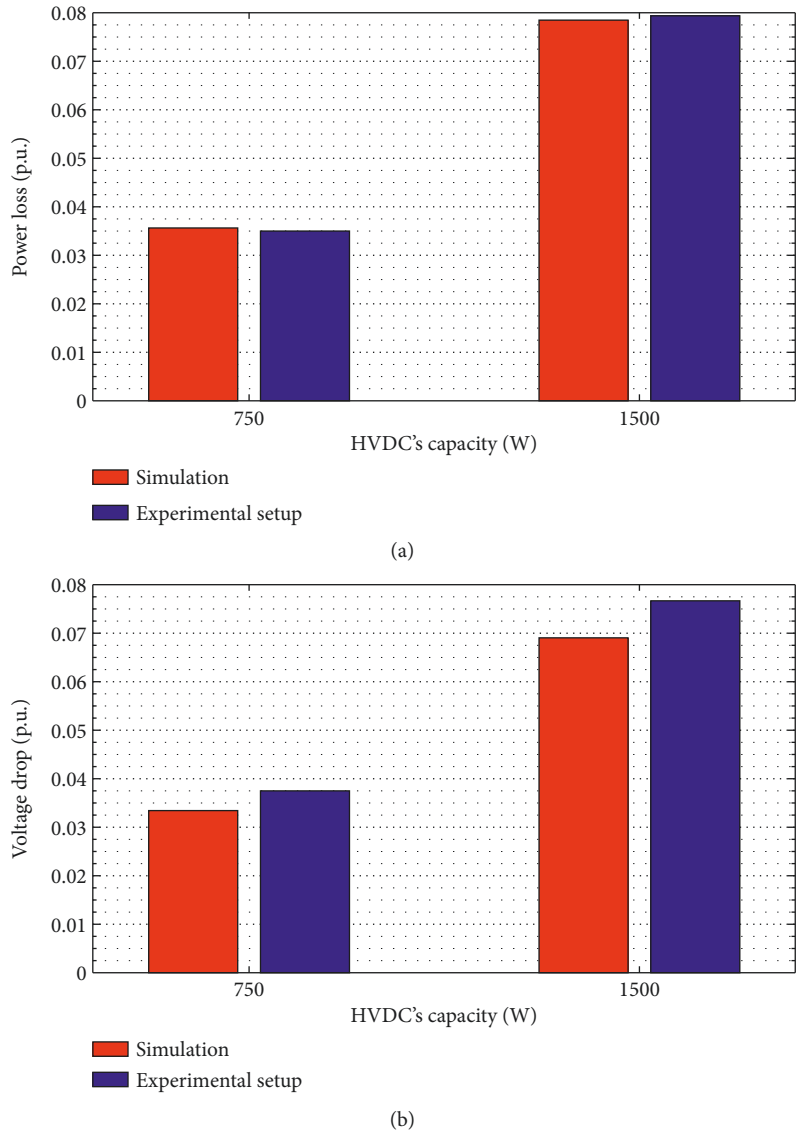

Figure 17: Comparison of the power losses and voltage drops based on the electrical load conditions. (a) Comparison of the power losses and (b) comparison of the voltage drops.

$$V_{\text{drop,line}} = V_{\text{Sen}} - V_{\text{Rec}}. \tag{6}$$

The $P_{\text{loss, line}}$ is the power loss of the HVDC transmission line, which is the difference between the active power of the sending side (P_{Sen}) and the active power of the receiving side (P_{Rec}). The $P_{\text{loss, line}}$ is also calculated using the line conductance of the HVDC transmission line (G) multiplied by the square of the voltage drop ($V_{\text{drop, line}}$). The voltage drop is the voltage difference between the voltages of the sending side (V_{Sen}) and the receiving side (V_{Rec}).

3.1. Transmission Line Distance Condition. The HVDC transmission line is considered in three distances: 150, 300, and 600 km. All the distances are tested based on a capacity of 500 V and 750 W. The electrical parameter is considered by both voltage and current waveforms at the sending side (Sen) and the receiving side (Rec) of the HVDC transmission line. The voltage and current waveforms of the MATLAB/Simulink program and the experimental setup are compared at different transmission line distances as shown in Figures 12 and 13.

The voltage waveforms in Figure 12 have vertical and horizontal axes as the voltage value (V) and operating time (s), respectively. The voltage waveforms are compared between the transmission line distances of 150 km, 300 km, and 600 km. However, the results of the simulation and the experimental setup are also analysed, in which the sending side of the transmission line is shown in Figure 12(a) and the receiving side of the transmission line is shown in Figure 12(b).

The comparison between the transmission line distances demonstrates that the waveforms of 600 km transmission line distance are the smoothest, whereas the 150 km and 300 km distances have more oscillation. Long transmission line spacing reduces the effect of voltage harmonics, where

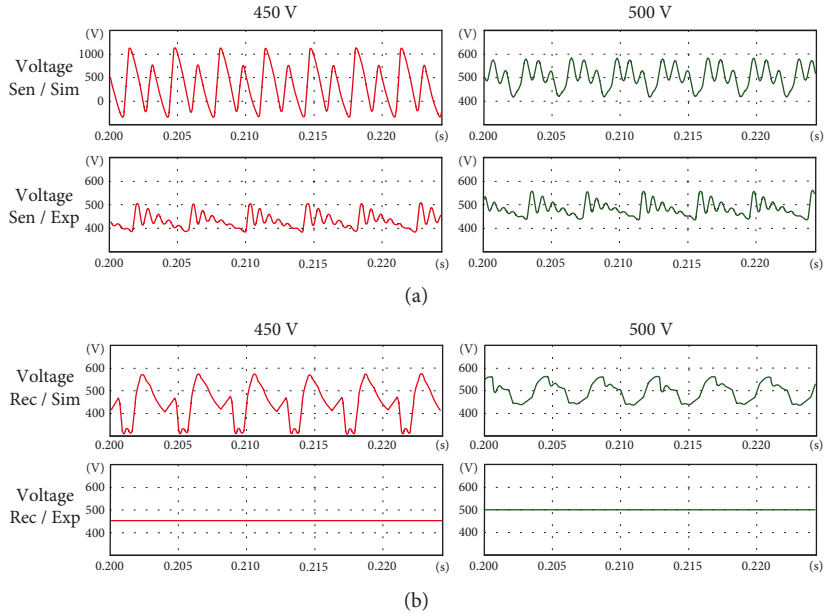

Figure 18: Comparison of the voltage waveforms based on the voltage conditions. (a) Comparison of the sending side current waveforms and (b) comparison of the receiving side voltage waveforms.

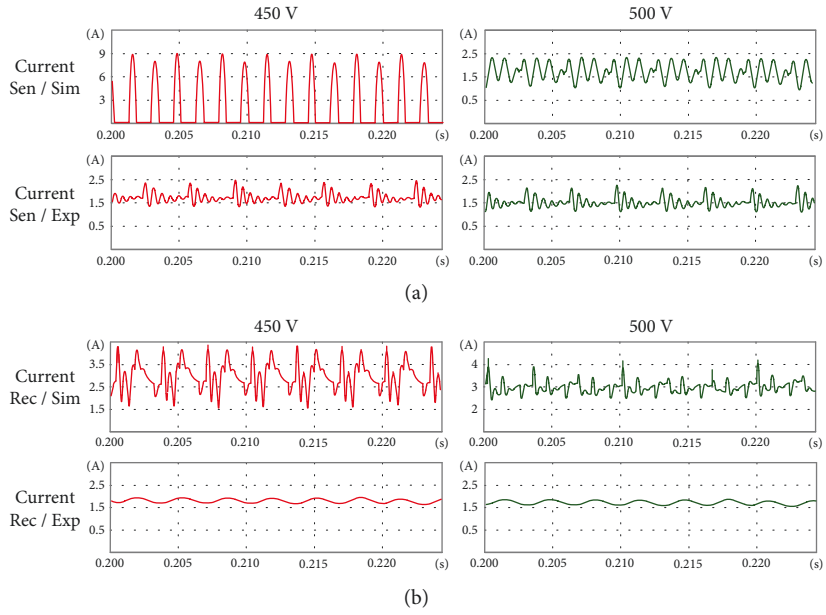

Figure 19: Comparison of the current waveforms based on the voltage conditions. (a) Comparison of the sending side current waveforms and (b) comparison of the receiving side current waveforms.

the impedance in a transmission line can behave to some extent like a power system filler circuit. However, this will result in higher power loss and voltage drop. The comparison of the voltage waveforms between the sending side (Figure 12(a)) and the receiving side (Figure 12(b)) shows that the voltage waveforms at the receiving side are generally the smoothest. This is because the voltage waveform on the receiving side is less oscillating than on the sending side. Moreover, the longer the transmission line distance, the lower the harmonic voltage on the receiver side. The simulation and experimental results have similar waveform characteristics; however, the experimental results demonstrate smoother waveforms and more noticeable DC properties. It was found that the voltage waveform of the simulation result was more oscillating than that of the experimental result due to the frequency limitation of recording devices of laboratory instruments that cover less frequencies and distances than the simulation.

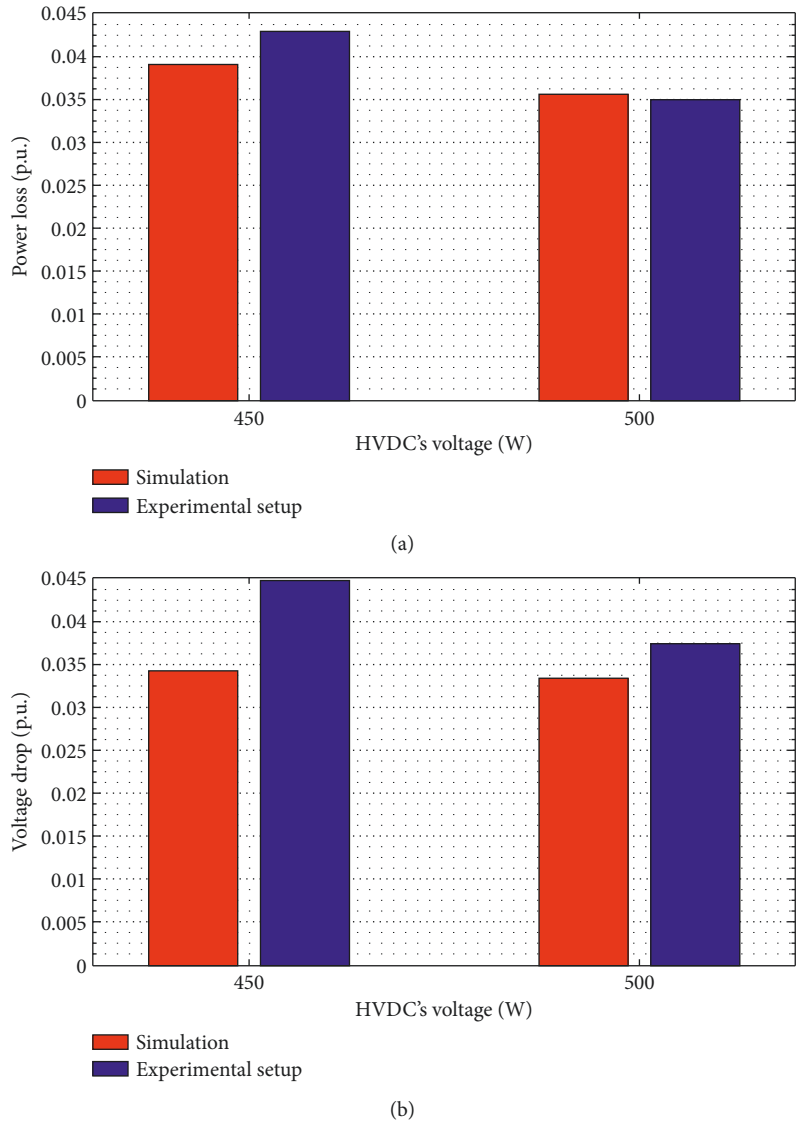

Figure 20: Comparison of the power losses and voltage drops based on the voltage conditions. (a) Comparison of the power losses and (b) comparison of the voltage drops.

Table 7: Summary of the results of the experiment according to the conditions.

Conditions		Results	
Parameter	Trend	Parameter	Trend
Transmission line distance	Increase	Power loss Voltage drops	Increase Increase
Load power	Increase	Power loss Voltage drops	Increase Increase
Transmission line voltage	Increase	Power loss Voltage drops	Uncertain Uncertain

The current waveforms shown in Figure 13 have vertical and horizontal axes as the current value (A) and operating time (s), respectively. The results are organized in the same manner as in Figure 13. It is found that the 600 km distance has the smoothest waveform, whereas the other distances have more oscillation. The current waveforms at the receiving side (Figure 13(b)) are smoother than those at the sending side (Figure 13(a)), and both the simulation and the experimental setup provide similar waveform characteristics.

The corresponding power loss and voltage drop are measured and analysed in Figure 14. The results demonstrate that the longer the transmission line distance, the higher the transmission line impedance and the greater the power loss as shown in Figure 14(a). Because the HVDC transmission line distance is doubled, the power loss and voltage drop are twice higher. The results of the MATLAB/Simulink program and the experimental setup show the same tendency. The power loss and voltage drop of both systems have similar values, but the simulated ones are slightly lower as shown in Figure 14(b) because of the impedance in the experimental wiring. This denotes that the power loss and voltage drop are directly proportional to the HVDC transmission line distance owing to the line's impedance.

3.2. Electrical Load Condition. The electrical load is studied under two conditions: 750 and 1500 W. Both conditions are tested with a voltage of 500 V and a distance of 600 km. The voltage and current waveforms at the sending and receiving sides of the HVDC transmission line are compared for the different electric load powers as shown in Figures 15 and 16.

The voltage waveforms in Figure 15 have vertical and horizontal axes as the voltage value (V) and operating time (s), respectively. The voltage waveforms are compared between the electrical loads of 750 W and 1500 W. However, the results of the simulation and the experimental setup are also analysed, in which the sending side of the transmission line is shown in Figure 15(a) and the receiving side of the transmission line is shown in Figure 15(b).

In Figure 15, the waveforms of the 750 W load are very much similar to those of the 1500 W load in both the simulation and experimental results because the change in load power does not affect the impedance in the transmission line but will result in more power loss due to more current flowing through the transmission line. A comparison of the voltage waveforms between the sending and the receiving sides shows that the voltage waveforms at the receiving side are generally smoother. However, the waveforms of the 1500 W load at the receiving side sway the most.

The current waveforms shown in Figure 16 have vertical and horizontal axes as the current value (A) and operating time (s), respectively. The 750 W and 1500 W loads have the same characteristics, whereas the 1500 W load has a higher current value. The current waveforms at the receiving side are smoother than those at the sending side, and the experimental setup results are smoother than the simulation results.

The corresponding power losses and voltage drops are shown in Figure 17. The simulation and experimental results show the same tendency: The higher the electrical load, the higher the current and the greater the power loss as shown in Figure 17(a). When the electrical loads are doubled, the power losses increase 2 times (in pu unit). The power loss in the experimental setup is similar to that in the simulation. The voltage drops of both systems have similar values; however, the simulated ones are slightly lower as shown in Figure 17(b). As the electrical loads are doubled, the voltage drops are twice higher. However, when considering the results of the simulation and the experimental setup, it was found that the experimental setup involved a number of external elements such as cables, terminals, and electrical protection devices. This results in a slightly greater power loss and voltage drop than those in the simulation.

3.3. Voltage Condition. The 450 V and 500 V voltage conditions are considered in this subsection. Both conditions are tested based on a capacity of 750 W and a distance of 600 km. The voltage and current waveforms at the sending and receiving sides of the MATLAB/Simulink program and the experimental setup are compared at different voltage conditions as shown in Figures 18 and 19. The voltage and current waveforms of the 450 V and 500 V voltage conditions are very similar in both systems; nevertheless, the receiving side has smoother waveforms than the sending side. Moreover, in the 450 V simulated system, the voltage and current waveforms are more oscillating. This may be the result of the rectifier's limited ability to adjust the voltage.

The results are compared in two aspects: the power loss and voltage drop. It is observed that the 450 V model has higher power losses than the 500 V model because at the same load power, the lower the voltage, the greater the current and power loss as shown in Figure 20(a). The voltage drops of both systems have similar values in both conditions as shown in Figure 20(b). Because the voltage conditions are not much different, the effects on voltage drops are rather small.

From the three subsection tests, the preliminary results showed that the power loss and voltage drop are directly proportional to the length of the HVDC transmission line because of the resistance of the line, whereas the power of the load is directly proportional to the power loss and voltage drop as well due to the greater current flowing through the power line. Yet, the change in transmission line voltage has no significant effect on the transmission line system as shown in Table 7.

4. Conclusion

This study focuses on the effect of transmission line distance, load power, and voltage on power loss, voltage drop, and waveform using the MATLAB/Simulink program and the experimental setup for consideration of preventing damage to the HVDC system. The results show that the longer the transmission line distance, the higher the transmission line impedance and the greater the power loss. The power loss and voltage drop are directly proportional to the HVDC transmission line distance because of the line's impedance. For the different load power conditions, the higher the electrical load, the higher the current and the greater the power loss. The increase in the power loss is many times greater than that in the load power. The power loss and voltage drop of both systems have similar values. Finally, for the different voltage conditions, the effects on power loss and voltage drop are rather small because the voltage conditions are not much different. Nevertheless, the waveforms of the 450 V model show more pronounced oscillation. This may

be as a result of the rectifier's limited ability to adjust the voltage. This study can be used to describe the electrical phenomena of an HVDC transmission line in a real system under the effects of each condition. The results of this study can be applied to the design of high-voltage direct current transmission lines. In addition, it is also possible to simulate the power transmission conditions according to the design to consider the impact before the actual construction and estimate the impact of renewable energy and faults in the HVDC transmission line.

Data Availability

No data were used to support this study.

Conflicts of Interest

The authors declare that they have no conflicts of interest regarding the publication of this paper.

Acknowledgments

The work is part of a research project (no. A118-0361-030) sponsored by the King Mongkut's Institute of Technology Ladkrabang Research Fund. The author would like to thank them for their financial support.

References

[1] G. Cordioli, D. Retzmann, and K. Uecker, *Benefit of HVDC for System Intersection*, Energy Sector SIEMENS Power Transmission Division, 2008.

[2] S. Chakraborty, P. K. Sadhu, and N. Pal, "HVDC application for different solar PV technology combinations in India," *TELKOMNIKA Indonesian Journal of Electrical Engineering*, vol. 12, no. 12, 2014.

[3] C. Humpert and Christof, "Long distance transmission systems for the future electricity supply – analysis of possibilities and restrictions," *Energy*, vol. 48, no. 1, pp. 278–283, 2012.

[4] S. P. Ramezanzadeh, M. Mirzaie, and M. Shahabi, "Reliability assessment of different HVDC transmission system configurations considering transmission lines capacity restrictions and the effect of load level," *International Journal of Electrical Power & Energy Systems*, vol. 128, Article ID 106754, 2021.

[5] X. Chu, "Unbalanced current analysis and novel differential protection for HVDC transmission lines based on the distributed parameter model," *Electric Power Systems Research*, vol. 171, pp. 105–115, 2019.

[6] S. Sanchez, A. Garcés, G. Bergna-Diaz, and E. Tedeschi, "Dynamics and stability of meshed multiterminal HVDC networks," *IEEE Transactions on Power Systems*, vol. 34, no. 3, pp. 1824–1833, 2019.

[7] Department of Alternative Energy Development and Efficiency, *Renewable Energy Performance of Jan-Nov 2016 and Oct-Nov 2016*, Ministry of Energy, 2017.

[8] J.-P. Sawicki, P. Petit, A. Zégaoui, M. Aillerie, and J.-P. Charles, "High efficiency step-up HVDC converter for photovoltaic generator," *Energy Procedia*, vol. 18, pp. 1593–1600, 2012.

[9] R. Radzuan, M. A. A. Raop, M. K. M. Salleh, M. K. Hamzah, and R. A. Zawawi, "The Designs of Low Power AC-DC Converter for Power Electronics System Applications," in *Proceedings of the 2012 International Symposium on Computer Applications and Industrial Electronics*, pp. 113–117, Kota Kinabalu, Malaysia, December 2012.

[10] M. Barnes and A. Beddard, "Voltage source converter HVDC links – the state of the art and issues going forward," *Energy Procedia*, vol. 24, pp. 108–122, 2012.

[11] O. E. Oni, I. E. Davidson, and K. N. I. Mbangula, "A Review of LCC-HVDC and VSC-HVDC Technologies and Applications," in *Proceedings of the 2016 IEEE 16th International Conference on Environment and Electrical Engineering*, pp. 1–7, Florence, Italy, June 2016.

[12] K. Friedrich, "Modern HVDC PLUS application of VSC in modular multilevel converter topology," in *Proceedings of the 2010 IEEE International Symposium on Industrial Electronics*, pp. 3807–3810, Bari, Italy, July 2010.

[13] B. Jacobson, P. Karlsson, G. Asplund, L. Harnefors, and T. Jonsson, "VSC-HVDC transmission with cascaded two-level converters," *CIGR´E B4*, vol. 110, 2010.

[14] D. Jovcic, L. Lamont, and K. Abbott, "Control system design for VSC transmission," *Electric Power Systems Research*, vol. 77, no. 7, pp. 721–729, 2007.

[15] Y. Xue, D. Kong, Z. Song, V. Hamidi, and X. Zhang, "Development of an Advanced LCC-HVDC Model for Transmission System," in *Proceedings of the 11th IET International Conference on AC and DC Power Transmission*, pp. 1–5, Birmingham, February 2015.

[16] H. Lan, T.-g. Yuan, M.-Z. Zhang, and Z.-m. Liao, "HVDC Intelligent Controller, Energy Procedia," *HVDC intelligent controller*, vol. 17, pp. 1460–1467, 2012.

[17] H. Xiao, K. Sun, J. Pan, Y. Li, and Y. Liu, "Review of hybrid HVDC systems combining line communicated converter and voltage source converter," *International Journal of Electrical Power & Energy Systems*, vol. 129, Article ID 106713, 2021.

[18] T. Pakorn, R. Dietmar, O. Emmanuel, and W. Markus, "Smart Transmission System by HVDC and FACTS," in *Proceedings of the 2013 IEEE Grenoble Conference*, pp. 1–6, Grenoble, France, June 2013.

[19] Y. Zhang, J. Ravishankar, J. Fletcher, R. Li, and M. Han, "Review of modular multilevel converter based multi-terminal HVDC systems for offshore wind power transmission," *Renewable and Sustainable Energy Reviews*, vol. 61, pp. 572–586, 2016.

[20] H. Pang, G. Tang, and Z. He, "Evaluation of losses in VSC-HVDC transmission system," in *Proceedings of the IEEE Power and Energy Society General Meeting - Conversion and Delivery of Electrical Energy in the 21st Century*, pp. 1–6, Pittsburgh, PA, USA, July 2008.

[21] M. Dinh, S. Kim, J. Kim, M. Park, I. Yu, and B. Yang, "Loss characteristic analysis of an HTS DC model cable connected to a model VSC-HVDC system," *IEEE Transactions on Applied Superconductivity*, vol. 23, no. 3, Article ID 5900305, 2013.

[22] C. K. Gan, Y. M. Lee, D. Pudjianto, and G. Strbac, "Role of Losses in Design of DC cable for Solar PV Applications," in *Proceedings of the 2014 Australasian Universities Power Engineering Conference (AUPEC)*, pp. 1–5, Perth, WA, Australia, October 2014.

[23] F. M. Kasangala and G. Atkinson-Hope, "Electrical energy losses and costs evaluation of HVDC and UHVDC transmission lines," in *Proceedings of the 10th Industrial and Commercial Use of Energy Conference*, pp. 1–7, Cape Town, South Africa, August 2013.

[24] F. Yin, M. Farzaneh, and X. Jiang, "A finite element approach to calculate corona losses on bipolar DC transmission lines," in *Proceedings of the 2015 IEEE Conference on Electrical*

Insulation and Dielectric Phenomena (CEIDP), pp. 423–426, Ann Arbor, MI, USA, October 2015.

[25] F. Wang, Z. Xu, Y. Huang, and X. Li, "DC Harmonic Current Calculation for HVDC Systems Based on the Classical Transmission Line Model," in *Proceedings of the 2010 International Conference on Power System Technology*, pp. 1–5, Zhejiang, China, October 2010.

[26] T. Senjyu, K. Kurohane, J. Miyagi, and N. Urasaki, "Low-loss HVDC transmission system with self-commutated power converter introducing zero-current soft-switching technique," *IET Generation, Transmission & Distribution*, vol. 3, no. 4, pp. 315–324, 2009.

[27] I. Sanz, M. Moranchel, S. Fernández, F. J. Rodríguez, and J. Pérez, "Reconfiguration Algorithm to Reduce Power Losses in Offshore HVDC Transmission Lines," in *Proceedings of the 2014 International Conference on Renewable Energy Research and Application (ICRERA)*, pp. 524–528, Milwaukee, WI, USA, October 2014.

[28] M. You, B. H. Zhang, L. Y. Cheng, Z. Q. Bo, and A. Klimek, "Lightning Model for HVDC Transmission Lines," in *Proceedings of the 10th IET International Conference on Developments in Power System Protection (DPSP 2010)*, pp. 1–5, Managing the Change, Manchester, April 2010.

[29] M. Khatir, S. A. Zidi, M. K. Fellah, S. Hadjeri, and O. Dahou, "HVDC transmission line models for steady-state and transients analysis in SIMULINK environment," in *Proceedings of the IECON 2006-32nd Annual Conference on IEEE Industrial Electronics*, pp. 436–441, Paris, France, November 2006.

[30] A. Moharana, R. Varma, and R. Seethapathy, "Modal Analysis of Type-1 Wind Farm Connected to Series Compensated Transmission Line and LCC HVDC Transmission Line," in *Proceedings of the 2012 IEEE Electrical Power and Energy Conference*, pp. 202–209, London, ON, Canada, October 2012.

[31] X. Zhang, J. Bai, G. Cao, and C. Chen, "Optimizing HVDC control parameters in multi-infeed HVDC system based on electromagnetic transient analysis," *International Journal of Electrical Power & Energy Systems*, vol. 49, pp. 449–454, 2013.

[32] X. Cao, S. Wang, and L. Chen, "Overvoltage Study of a Real HVDC Project Based MATLAB," in *Proceedings of the 2013 IEEE 7th International Power Engineering and Optimization Conference (PEOCO)*, pp. 66–70, Langkawi, Malaysia, June 2013.

[33] Z. Haibo, F. Gruson, D. Florez, and C. Saudemont, "Analysis of the Influence of Different cable Modelling for DC Series Offshore Wind Farm," in *Proceedings of the 2016 18th European Conference on Power Electronics and Applications (EPE'16 ECCE Europe)*, pp. 1–9, Karlsruhe, Germany, September 2016.

[34] S. Akkari, E. Prieto-Araujo, J. Dai, O. Gomis-Bellmunt, and X. Guillaud, "Impact of the DC cable Models on the SVD Analysis of a Multi-Terminal HVDC System," in *Proceedings of the 2016 Power Systems Computation Conference (PSCC)*, pp. 1–6, Genoa, Italy, June 2016.

[35] A. Beddard and M. Barnes, "HVDC cable Modelling for VSC-HVDC Applications," in *Proceedings of the IEEE PES General Meeting | Conference & Exposition*, pp. 1–5, National Harbor, MD, USA, July 2014.

[36] J. Sabatier, T. Youssef, and M. Pellet, "HVDC Line Parameters Estimation Based on Line Transfer Functions Frequency Analysis," in *Proceedings of the 2015 12th International Conference on Informatics in Control, Automation and Robotics (ICINCO)*, pp. 497–502, Colmar, France, June 2015.

[37] P. Liu, R. Che, Y. Xu, and H. Zhang, "Detailed Modeling and Simulation of +500kV HVDC Transmission System Using PSCAD/EMTDC," in *Proceedings of the 2015 IEEE PES Asia-Pacific Power and Energy Engineering Conference (APPEEC)*, pp. 1–3, Brisbane, QLD, Australia, November 2015.

[38] Z. Zhang, X. Qiao, S. Yang, and X. Jiang, "Non-uniform distribution of contamination on composite insulators in HVDC transmission lines," *Applied Sciences*, vol. 8, no. 10, 2018.

[39] D. Wang, T. Lu, X. Li et al., "Simulation and analysis of human body micro-shocks in the ion flow field near HVDC transmission lines," *Journal of Electrostatics*, vol. 93, pp. 10–16, 2018.

[40] J. Liao, N. Zhou, and Q. Wang, "DC-side harmonic analysis and DC filter design in hybrid HVDC transmission systems," *International Journal of Electrical Power & Energy Systems*, vol. 113, pp. 861–873, 2019.

[41] Y. Cui, X. Song, C. Wang, L. Zhao, and G. Wu, "Ground-level DC electric field sensor for overhead HVDC/HVAC transmission lines in hybrid corridors," *IET Generation, Transmission & Distribution*, vol. 14, no. 19, pp. 4173–4178, 2020.

[42] Y. Liu, Y. Liu, Y. Cui, H. Yuan, and J. Lv, "Analysis of the relationship between DC component and spectral components of corona current on HVDC transmission lines," *IET Generation, Transmission & Distribution*, vol. 13, no. 10, pp. 1952–1959, 2019.

[43] M. Marzinotto, G. Mazzanti, and M. Nervi, "Ground/sea return with electrode systems for HVDC transmission," *International Journal of Electrical Power & Energy Systems*, vol. 100, pp. 222–230, 2018.

[44] C. Tejada-Martinez, F. P. Espino-Cortes, S. Ilhan, and A. Ozdemir, "Optimization of radio interference levels for 500 and 600 kV bipolar HVDC transmission lines," *Energies*, vol. 12, no. 16, 2019.

[45] M. Zhou, W. Xiang, W. Zuo, W. Lin, and J. Wen, "A novel HVDC circuit breaker for HVDC application," *International Journal of Electrical Power & Energy Systems*, vol. 109, pp. 685–695, 2019.

[46] E. Rodrigues, R. Pontes, J. Bandeira, and V. Aguiar, "Analysis of the incidence of direct lightning over a HVDC transmission line through EFD model," *Energies*, vol. 12, no. 3, p. 555, 2019.

[47] K. Zhu, W. K. Lee, and P. W. T. Pong, "Non-contact voltage monitoring of HVDC transmission lines based on electromagnetic fields," *IEEE Sensors Journal*, vol. 19, no. 8, pp. 3121–3129, 2019.

[48] B. Netisak, "HVDC transmission technology for a sustained power system," *Journal of the Faculty of Industrial Technology Lampang Rajabhat University*, vol. 4, no. 2, pp. 78–91, 2012.

[49] M. Farshad, "Detection and classification of internal faults in bipolar HVDC transmission lines based on K-means data description method," *International Journal of Electrical Power & Energy Systems*, vol. 104, pp. 615–625, 2019.

[50] Y. Ma, H. Li, G. Wang, and J. Wu, "Fault analysis and traveling-wave-based protection scheme for double-circuit LCC-HVDC transmission lines with shared towers," *IEEE Transactions on Power Delivery*, vol. 33, no. 3, pp. 1479–1488, 2018.

[51] R. Muzzammel, "Machine learning based fault diagnosis in HVDC transmission lines," in *Intelligent Technologies and Applications*, I. Bajwa, F. Kamareddine, and A. Costa, Eds., vol. 932, Singapore, 2019.

[52] B. Mitra, B. Chowdhury, and M. Manjrekar, "HVDC transmission for access to off-shore renewable energy: a review of technology and fault detection techniques," *IET Renewable Power Generation*, vol. 12, pp. 1563–1571, 2018.

[53] A. Saber, H. Zeineldin, T. El-Fouly, and A. Al-Durra, "Current differential relay characteristic for bipolar HVDC transmission line fault detection," *IET Generation, Transmission & Distribution*, vol. 14, no. 23, pp. 5505–5513, 2020.

[54] N. M. Haleem and A. D. Rajapakse, "Fault-type discrimination in HVDC transmission lines using rate of change of local currents," *IEEE Transactions on Power Delivery*, vol. 35, no. 1, pp. 117–129, 2020.

[55] Xu Chu and H. Lv, "Coupling characteristic analysis and a fault Pole detection Scheme for single-circuit and double-circuit HVDC transmission lines," *Electric Power Systems Research*, vol. 181, Article ID 106179, 2020.

[56] H. Shu, Na An, Bo Yang, Y. Dai, and Yu Guo, "Single Pole-to-Ground fault analysis of MMC-HVDC transmission lines based on capacitive fuzzy identification algorithm," *Energies*, vol. 13, no. 2, p. 319, 2020.

[57] X. Zheng, M. H. Nadeem, N. Tai et al., "A transient current protection and fault location scheme for MMC-HVDC transmission network," *International Journal of Electrical Power & Energy Systems*, vol. 124, Article ID 106348, 2021.

[58] J. Duan, H. Li, Y. Lei, and L. Tuo, "A novel non-unit transient based boundary protection for HVDC transmission lines using synchrosqueezing wavelet transform," *International Journal of Electrical Power & Energy Systems*, vol. 115, Article ID 105478, 2020.

[59] Z. Dai, N. Liu, C. Zhang, X. Pan, and J. Wang, "A pilot protection for HVDC transmission lines based on transient energy ratio of DC filter link," *IEEE Transactions on Power Delivery*, vol. 35, no. 4, pp. 1695–1706, 2020.

[60] Y. Zhang, Y. Li, J. Song, X. Chen, Y. Lu, and W. Wang, "Pearson correlation coefficient of current derivatives based pilot protection scheme for long-distance LCC-HVDC transmission lines," *International Journal of Electrical Power & Energy Systems*, vol. 116, Article ID 105526, 2020.

[61] Y. Zhang, Y. Li, J. Song, B. Li, and X. Chen, "A new protection scheme for HVDC transmission lines based on the specific frequency current of DC filter," *IEEE Transactions on Power Delivery*, vol. 34, no. 2, pp. 1–429, 2018.

[62] J. Zheng, M. Wen, Yu Chen, and X. Shao, "A novel differential protection scheme for HVDC transmission lines," *International Journal of Electrical Power & Energy Systems*, vol. 94, pp. 171–178, 2018.

[63] M. Mehrabi-Kooshki, S. S. Mirhosseini, and S. Jamali, "Single-end protection algorithm for HVDC transmission lines based on the current difference," *IET Generation, Transmission & Distribution*, vol. 14, no. 20, pp. 4339–4351, 2020.

[64] M. Nandan, A. Pachori, and N. Saxsena, "HVDC transmission system using 6-pulse IGBT converter," *International Journal of Engineering Research and Development*, vol. 7, no. 7, pp. 37–44, 2013.

[65] S. Sayed and A. Massoud, "Minimum transmission power loss in multi-terminal HVDC systems: a general methodology for radial and mesh networks," *Alexandria Engineering Journal*, vol. 58, no. 1, pp. 115–125, 2019.